Aalto University
School of Electrical Engineering
Degree Programme in Nano and Radio Sciences

Badri Narayanan Narasimhan

Chemically programmed timing for nanocellulose colloidal gelation

Master's Thesis
Espoo, March 7, 2017

Supervisor: Professor Olli Ikkala
Instructor: Angel Sanchez Sanchez D.Sc. (Tech.)

Aalto University
School of Electrical Engineering
Degree Programme in Nano and Radio Sciences

ABSTRACT OF
MASTER'S THESIS

Author:	Badri Narayanan Narasimhan		
Title:	Chemically programmed timing for nanocellulose colloidal gelation		
Date:	March 7, 2017	**Pages:**	vii + 84
Professorship:	Engineering Physics	**Code:**	PHYS
Supervisor:	Professor Olli Ikkala		
Instructor:	Angel Sanchez Sanchez D.Sc. (Tech.)		

Cellulose nanofibrils (CNF) have generated great research interest due to their biocompatibility, sustainability and potential to build functional materials and devices with better mechanical properties. This work involves a chemically programmed timing method to form CNF hydrogels from aqueous colloidal suspensions by making use of slow hydrolysis reaction of glucono-δ-lactone (GdL) to gluconic acid. Fourier transform infrared spectroscopy and UV-Vis spectroscopy using cationic dye toluidine blue (TB) suggests that the gelation is driven by the supracolloidal crosslinking of the CNF nanofibrils by hydrogen bondings mediated by carboxylic acid dimerization. This results from the transition of the sodium carboxylate groups in the TEMPO oxidized CNF fibrils to carboxylic acids. Rheological experiments revealed that the concentration of GdL used to form hydrogels allows tuning of the gelation times from minutes to days. In addition, the storage modulus of the gels can be tuned by the amount of added GdL. Thus we envision that the chemically programmed timing concept allows the programming of processing window before the elastic gels are formed. The method also allowed a controlled introduction of redox active tetra(aniline) (TANI) onto the CNF hydrogels. The method is suggested to open up new possibilities for functional hydrogels, e.g. incorporating conductivity or electrochromic properties and making mechanically tough double gels.

Keywords:	nanocellulose, colloids, hydrogels, glucono-δ-lactone hydrolysis, toluidine blue
Language:	English

Acknowledgements

I would like to thank my advisor Dr.Angel Sanchez Sanchez for his friendly guidance throughout this project. The endless scientific discussions we had has really helped me a lot during the project and also will be helpful in future. My countless thanks for helping me out in difficult times and also for educating me in the right way.

My sincere thanks to my supervisor Professor Olli Ikkala.Thanks for the motivational discussions and your continuous involvement with the project. I learnt a great deal of science from you and also thanks for the comments you gave before my presentation.

I thank Dr.Sami Hietala for teaching me rheology and for patiently answering my questions. Prof. Charl Faul is acknowledged for providing oligo(aniline) and Teemu Myllymäki is acknowledged for providing carbon nanotubes. I would like to thank all the members of Molmat for providing such a nice environment to work and also for the technical inputs you gave me. It was indeed nice to work with you people. I thank Martin for being a nice lab buddy to me. I would like to thank Nonappa and Nikolai for the coffee discussions.

My special thanks to my friends Narayani, Sathish and Sridhar for kindly putting up with me in all these years and the fun we had together. Finally I would like to thank my dad, grandma and my family for supporting me inspite of completely different views we have in life.

Espoo, March 7, 2017

Badri Narayanan Narasimhan

Abbreviations and Acronyms

CNF	Cellulose nanofibers, i.e. nanofibrillated cellulose
CNC	Cellulose nanocrystals
GdL	Glucono-δ-lactone
TEMPO	2,2,6,6-tetramethylpiperidine-1-oxyl radical
PANI	Poly(aniline)
TANI	Tetra(aniline)
CNT	Carbon nanotubes
FWCNT	Few walled carbon nanotubes
SEM	Scanning electron microscopy
TEM	Transmission electron microscopy
FTIR	Fourier transform infrared spectroscopy
UV-Vis-NIR	Ultraviolet visible near infrared
TB	Toluidine blue
PEDOT: PSS	Poly(3,4-ethylenedioxythiophene) polystyrene sulfonate

Contents

Chapter 1

Introduction

The search to use low cost sustainable material resources has recently created a strong research interest towards using biopolymers, such as cellulose, for high tech materials and device applications. To enable mass production, cheap manufacturing methodologies are needed, like paper making [1] and printing technologies [2]. Hydrogels are water-based network materials, and they are interesting candidates for functional materials, as they can be made biocompatible [3] and can serve as mimics of biological environment. Hydrogels can possess high ion mobility and can provide charge-transport selectivity [4]. The construction of devices based on the control of flow of ions is called iontronics. The use of iontronic devices will tackle the fundamental limitations posed by organic electronics devices such as efficiency limited by dimensions and low conductivity which hinders their use in daily life applications [4]. Therefore, iontronic devices have potential applications in neuromorphic circuits [5–7], biosensors [8] and energy applications [9–11].

As mentioned, in addition to identify low cost sustainable materials, there is also a need to produce devices which are sustainable. The reason is due to the waste generated, e.g, by electronic devices, where the so called e-waste leads to environmental pollution and adverse health effects [12]. It is estimated that the e-waste volume generated globally is increasing at the rate of 5-10 % yearly [13]. In developing countries like India, the e-waste production is estimated to be 1.25 million metric tons per annum and is likely to increase to 1.5 million metric tons [14]. Thus, current scientific efforts have been focused on the investigation of biodegradable and sustainable materials with interesting physical properties to allow device options.

Organic based devices can offer sustainable approach to produce devices with low energy consumption for applications such as stretchable electronics [15] and biocompatible implantable biosensors [16] due to the properties of organic materials used in the devices. Nevertheless, these materials do not, as

such, show the desirable mechanical properties suitable for the applications mentioned. Therefore, biopolymer matrices have been utilized for making organic electronic devices with optimal mechanical properties. Among these biopolymers, cellulose has attractive features such as biocompatibility, sustainability, light weight and flexible and most importantly, available in abundance in countries like Finland [17–19].

Self-assembly due to competing interactions allows spontaneous control of structures for obtaining functional properties, such as transport properties [20]. Supramolecular chemistry is a bottom up approach to build self-assembled molecular structures based on intermolecular interactions. It was pioneered by Jean-Marie Lehn who defines supramolecular chemistry as 'Chemistry beyond the molecule' [21]. Supramolecular Chemistry has various applications such as producing self-healing materials [22] and in the production of colloidal hydrogels [23], etc. Self-assemblies combined with supramolecular concepts form the basis for the hydrogels described in this work.

The present work introduces chemical programming of nanocellulose-based hydrogels from aqueous colloidal dispersions. This is achieved by self-assembly of cellulose nanofibrils by controlling the pH by adding a gel activator. The self-assembly process is monitored and controlled with time. The mechanical properties of the produced hydrogels are tuned by controlling the amount of the gel activator. A chemical programming based approach to incorporate conducting molecules and colloids inside hydrogels is developed. Finally, the potential for building iontronic devices out of the preparation method is sketched. In the introduction part, a brief introduction about nanocellulose is described. This is followed by description of physical interactions which drive the self-assembly of cellulose fibrils to form hydrogels. Then, preparation methods and properties of hydrogels and aerogels based on nanocellulose are described. A note on electroactive devices based on electrically conducting molecules is elaborated which gives an understanding of the state of the art preparation method used in this work.

Chapter 2

Background

2.1 Cellulose and nanocellulose

Cellulose is a polymer widely available from natural sources such as wood, cotton and plants. It has recently attracted considerable renewed attention as a biodegradable material from renewable source for a wide range of applications. Cellulose polymer chains consist of β-1,4-linked D-glucopyranose monomers [24]. They are arranged in linear chains in which the glucosidic oxygens point in the opposite directions to form *cellobiose units* [24, 25]. The physical and chemical properties of cellulose are strongly dependent on the arrangement of cellulose molecules in the crystal lattice.

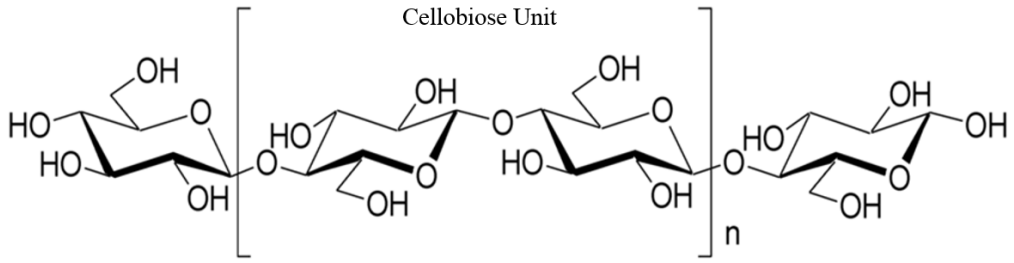

Figure 2.1: Molecular structure of cellulose generated from repeating β-D-glucopyranose molecules [26].

Cellulose has several crystalline structures. The polymorph found in nature is cellulose-I, also called as the native cellulose, incorporating parallel hydrogen bonded cellulose chains. Cellulose-II, III and IV are the other crystal structures of cellulose. Cellulose-II with its antiparallel chains shows higher thermodynamic stability. It is produced by treatment of cellulose-I

with aqeuous sodium hydroxide, the so called mercerization process or by dissolution of cellulose followed by precipitation [25].

Beyond individual cellulose molecular chains, nanocelluloses are colloidal nanofibers typically disintegrated from the hierarchical structure of plants or wood. Their lateral dimensions are in the range of nanometers and their length differs depending on the fabrication process. The major types of nanocelluloses are cellulose nanofibers (CNF), i.e. nanofibrillated cellulose (NFC), and cellulose nanocrystals (CNC). CNFs are nanofibrils produced by mechanical fibrillation processes, usually combined with chemical treatment or enzymatic processes [27]. CNF possesses length of 500-2000 nm and width of 4-20 nm. They have both amorphous and crystalline regions in a fringed micellar architecture. By contrast, CNCs are rod-like crystalline structures produced by strong acid hydrolysis of cellulose. CNC have width of 3-5 nm and length in the range of 50-500 nm [27].

Surface modifications of CNFs lead to improved disintegration from pulp and promoted processibility [28]. The reported synthetic procedures involve transformation of hydroxyl groups to functional groups such as aldehydes, ketones and carboxylates; to mention few examples [27, 28]. Among these chemistries, the most used method is the chemical modification of CNFs by a radical mediated oxidation, i.e., 2,2,6,6-tetramethylpiperidine-1-oxyl (TEMPO) oxidation. It is a simple and efficient procedure for surface carboxylation of native cellulose nanofibrils; Figure 2.2. When the native cellulose is treated with TEMPO/NaBr/NaClO in water at a pH of around 10 at room temperature, the C6 primary hydroxyls that are exposed on microfibril surfaces get selectively oxidized to carboxyls [29, 30]. The resulting oxidized cellulose fibrils dispersed in water are further subjected to mild mechanical disintegration treatment to obtain individualized nanofibrils with $\approx$4 nm width. The enhanced dispersibility of TEMPO oxidized cellulose nanofibrils is a consequence of repulsive forces between the anionically charged cellulose nanofibrils.

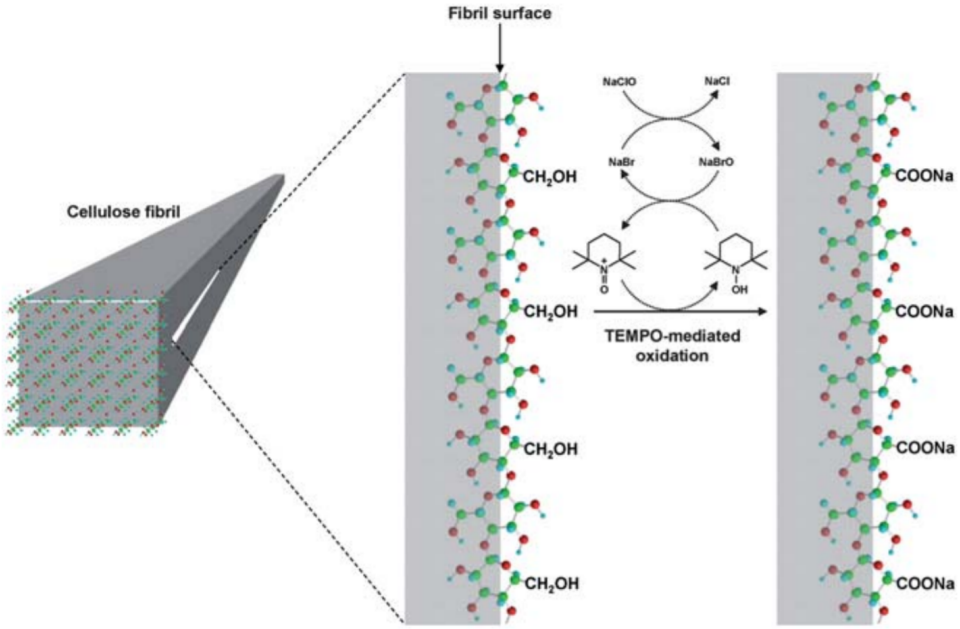

Figure 2.2: TEMPO oxidation of native cellulose fibrils [29].

2.2 Interesting properties of nanocellulose

Nanocelluloses possess several properties that make them potential candidates for composites and functional materials. The most important property deals with high mechanical stiffness and strength. For example, CNF films possess Young's modulus as high as 20 GPa [31] which can be used for making reinforced composite materials. Another interesting property demonstrated by CNC is the liquid crystalline behaviour and high electric dipole moments. The high dipole moments enables alignment by electric field [32].

2.3 Self-assembly

George M. Whitesides [33] defines self-assembly as 'the autonomous organization of components into patterns or structures without human intervention'. Self-assemblies form due to competing interactions, and typical examples of molecular self-assembly are liquid crystallinity, block copolymer structures, or protein folding and their hierarchical structures.

The competing interactions between the molecules can be formed using covalent or non-covalent interactions, such as van der Waals, hydrophobic, electrostatic, dipole-dipole, coordination, or $\pi - \pi$ stacking interactions, or hydrogen bonding. The ranges of these interactions vary widely [34]. Self-assemblies can take place using larger structural units, such as using nanocellulose, which are of colloidal scale. Noncovalent interactions can also allow self-assemblies into network materials, such as the CNF-based hydrogels, i.e. CNF networks in aqueous media.

2.4 Intermolecular interactions within cellulose nanofiber hydrogels

The intermolecular interactions are the driving forces for the CNF self-assembly towards colloidal physical networks. The networks manifest in the mechanical and viscoelastic properties [35]. In the following sections, hydrophobic interactions and hydrogen bonding interactions by CNF materials will be discussed as they contribute essentially to this work.

2.4.1 Hydrophobic interactions

Hydrophobic interactions form in aqueous phases to maximize the internal hydrogen bonds within water molecules and reduce the nonpolar molecular contacts with the polar water phase [36]. Thus, hydrophobic interactions can be described as an attractive force which brings the hydrophobic species to associate, such as into micelles and vesicles. The attraction brings the hydrophobic species together which makes the total volume of the hydrophobic species in contact with the solvent lesser than they are far apart; Figure 2.3.

(a) (b)

Figure 2.3: Two hydrophobic molecules. (a) Far apart (b) Closer due to hydrophobic interactions. The volume in contact with solvent is lesser in this case.

The balance between hydrophobic and hydrophilic interactions controls the observed physical structures and properties. Hydrophobic interactions also affect the swelling of the network chains in physically crosslinked gels [3]. In CNF, the amphiphilic nature of nanocellulose strongly affects the aqueous dispersibility due to the hydrophobic domains [37].

2.4.2 Hydrogen bonding interactions

According to Margaret C. Etter [38] 'a hydrogen bond is defined as an interaction that directs the association of a covalently bound hydrogen atom with one or more atoms or molecules into an aggregate structure that is sufficiently stable to make it convenient for the chemist to consider it as an independent chemical species'. The hydrogen bonding interaction is usually represented as

$$D - H \ldots A$$

where D stands for hydrogen bonding donor and A stands for acceptor atom. Classic hydrogen bonds are the directional interaction in water between O (O acts as an acceptor A here) and H-O groups (here O acts as a donor D). Hydrogen bond interactions incorporate of several types of contributions, such as electrostatic and dipolar forces, and their strength can vary widely [39]. The hydrogen bonding interactions are directional which is helpful in building stable structures. The available bonding geometry affects the strength. For example, in polypeptides and proteins, the hydrogen bonds in parallel β-sheets are nonlinear strained leading to weaker hydrogen bondings whereas antiparallel β-sheets are non-strained linear leading to stronger hydrogen bondings; Figure 2.4.

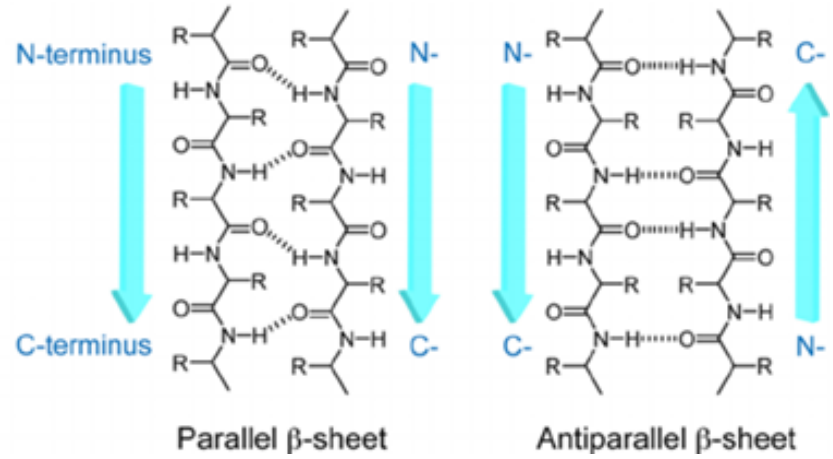

Figure 2.4: Parallel and anti-parallel arrangements of a monomeric actins [40].

The strength of hydrogen bonds ranges from 4 kJ/mol to 120 kJ/mol and it is greater than van der Waals interactions [41]. Hydrogen bonding interactions can also be intramolecular. The hydrogen bonding interactions can give rise to 1D, 2D or 3D structures due to the directionality of the bonds [42].

In molecular chains of cellulose, due to the presence of abundant -OH groups there is an ability to form both intra and intermolecular hydrogen bondings. They are the reason for the observed crystallization of cellulose [24]. They are also the major contributor to the insolubility of the cellulose in addition to hydrophobic interactions [42]. Now that we understand what is molecular self-assembly and its driving forces we will discuss some preparation methods where self-assembly is utilized in CNF-based materials.

Wang et al [43] used ionic assembly between anionic carboxymethylated CNF and cationic amphiphilic diblock copolymer micelles for building biomimetic composites. The scheme of self-assembly is shown in Figure 2.5. The advantage of this method is that it combines hard and soft architecture in the nanoscale and pave way for controlling the mechanical properties.

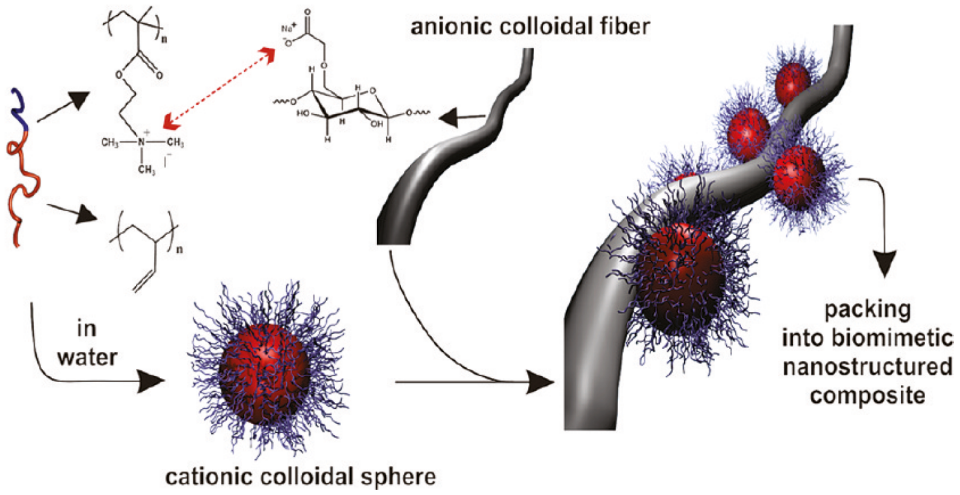

Figure 2.5: Scheme of ionic self-assembly. Ionic complexation between cationic quaternized poly(1,2-butadiene)-block-poly(dimethylaminoethyl methacrylate) micelles with anionic CNF [43].

Carbon nanotubes (CNT) are used as gate materials in transistors and light emitting diodes to enable flexibility and optical transparency. However,the protruding tubes of CNT results in electrical shorting in such devices. Huang et al [44] utilized hydrogen bonding interactions in addition to van der Waals interctions acting between CNF nanopaper and CNT arising due to the rich surface functional groups of CNF to produce flexible organic field effect transistors (OFET). CNTs adhere to the fibrillar surface resulting in the reduction of protruding tubes. In addition, the SEM revealed that the CNF nanopaper self-assemble into layer-by-layer structure; Figure 2.6. The advantage of this structure is that the strain gets released when the paper is bent enabling good flexibility. The nanopaper transistor also exhibited high smoothness, higher transmittance and better electrochemical properties. This shows potential use for producing flexible electronic devices.

The above examples show that by playing with intermolecular interactions and self-assembly one can tailor materials to suit different applications.

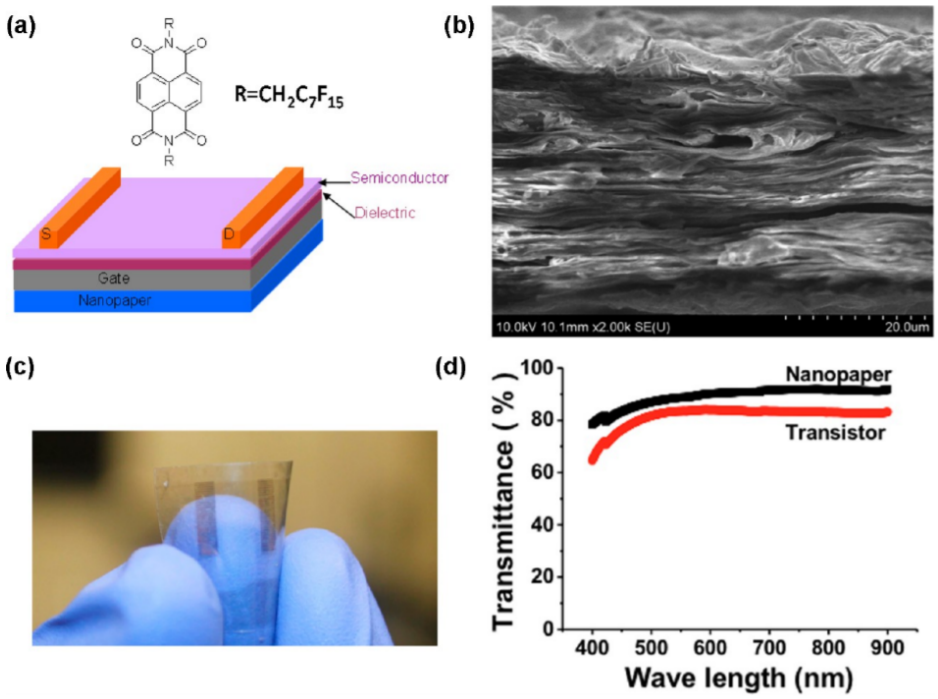

Figure 2.6: (a) Schematic of OFET (b) SEM indicating a smooth surface for the nanopaper transistor (c) Picture of fabricated transparent transistor (d) Optical transmittance of nanopaper and transistor at 550 nm [44].

2.5 Cellulose nanofiber hydrogels

This section will give introduction to hydrogels and aerogels followed by specific examples thereof using CNF. Hydrogels are networks in aqueous media. Hydrogels can be formed by chemical crosslinking chains as well as by physical association of starting materials as precursors to networks. Chemical or covalent crosslinking refers to the formation of permanent junctions, i.e. formation of new intramolecular covalent bonds, while physical association refers to the formation of transient junctions, i.e. association of network chains because of non-covalent interactions [45]. The gel network can also emerge due to the entanglement of the chains. The networks can be molecular or colloidal. In the case of CNF, physical colloidal hydrogels are produced in various forms depending on the concentration and physical crosslinks [46, 47]. There is a critical concentration above which the non-covalent interactions, such as hydrogen bondings and hydrophobic interactions, induce gelation. This critical concentration is referred as gel point. In the case of native CNF, the critical concentration is about 0.1%.

Another approach to form CNF gels with non-covalent interactions exploits the chemical surface functionalization of CNF. For instance, Saito et al [48] reported the formation of a CNF-based gel from initially well-dispersed colloidal suspensions of TEMPO-oxidized CNF, which involved carboxylate salt groups exposed on the CNF surfaces. The proposed mechanism for the formation of CNF gel involves the formation of new transient junctions, i.e. hydrogen bonding interactions, upon change of pH. The adjustment of pH with HCl produces the protonation of the carboxylate groups (around pKa 4.5) from the salt form to result in neutral carboxylic group at the surface of the cellulose fibril surface. These new electrically neutral functionalities reduce dispersibility in water properties in comparison to the anionically charged moieties, which leads to CNF networks with higher degree of association. Hydrogels obtained from TEMPO-CNF suspensions were reported to be quite handleable and stiff. The hydrogels showed a power law relation to storage modulus with an increase of CNF concentration.

Also addition of metal cations to carboxylated CNFs resulted in associations in the cellulose chains; Figure 2.7. The ionic interactions screen the repulsion between the negatively charged CNF and resulted in hydrogels [49, 50]. The storage moduli of the gels showed properties dependent on the valency of the metal cations. The observed storage moduli for the ionically crosslinked CNFs were in the range of 32 to 3.2 kPa.

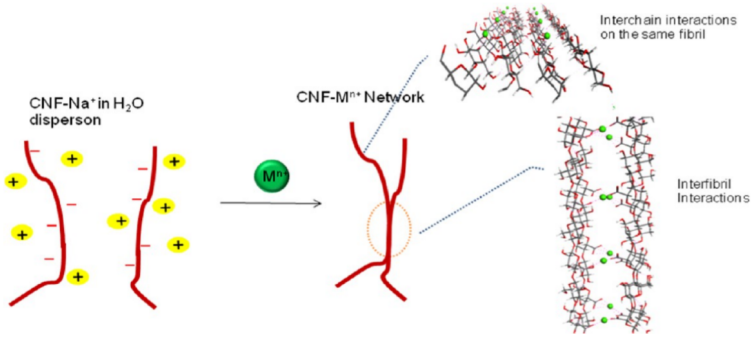

Figure 2.7: CNFs crosslinking with metal cations [49]

2.6 Cellulose nanofiber aerogels

Aerogels are derivatives of hydrogels in which the liquid component of gel is replaced with gas. The common methods to prepare aerogels are by freeze drying, solvent exchange and drying, and supercritical drying.

In freeze drying, the hydrogel is immersed in vacuum, leading to freezing and water sublimation, or immersed first in cryogenic fluid (e.g. liquid nitrogen) for freezing and sublimation. Liquid propane can also be used in place of liquid nitrogen. The difference is that liquid nitrogen produces sheet-like aggregates while liquid propane resulted in fibril-like aggregation [51]. Solvent exchange makes use of exchanging the water within the hydrogels with different solvents such as methanol and tert-butyl alcohol followed by freeze drying. Rapid initial cryogenic freezing step allows preservation of the fibrillar structure as it suppresses the growth of ice crystals to some extent [52]. Supercritical drying makes use of high temperature and high pressure to remove the liquid component from the hydrogels. It was shown that supercritical drying produced aerogels without major aggregation of fibrils [51].

Aerogels have potential applications in producing lightweight materials with thermal insulation. CNF aerogels have the advantages of good mechanical properties and relatively high surface area. Aerogels made out of 0.4% CNF prepared by addition of HCl showed elastic modulus of 64 kPa and surface area of 349 m^2g^{-1}; Figure 2.8.

CNF aerogels with conducting polymers finds potential use in building supercapacitors and sensors [53]. Thus, hydrogels and aerogels of CNF has potential in building functional composites which shows anisotropy, mechanical strength and flexibility.

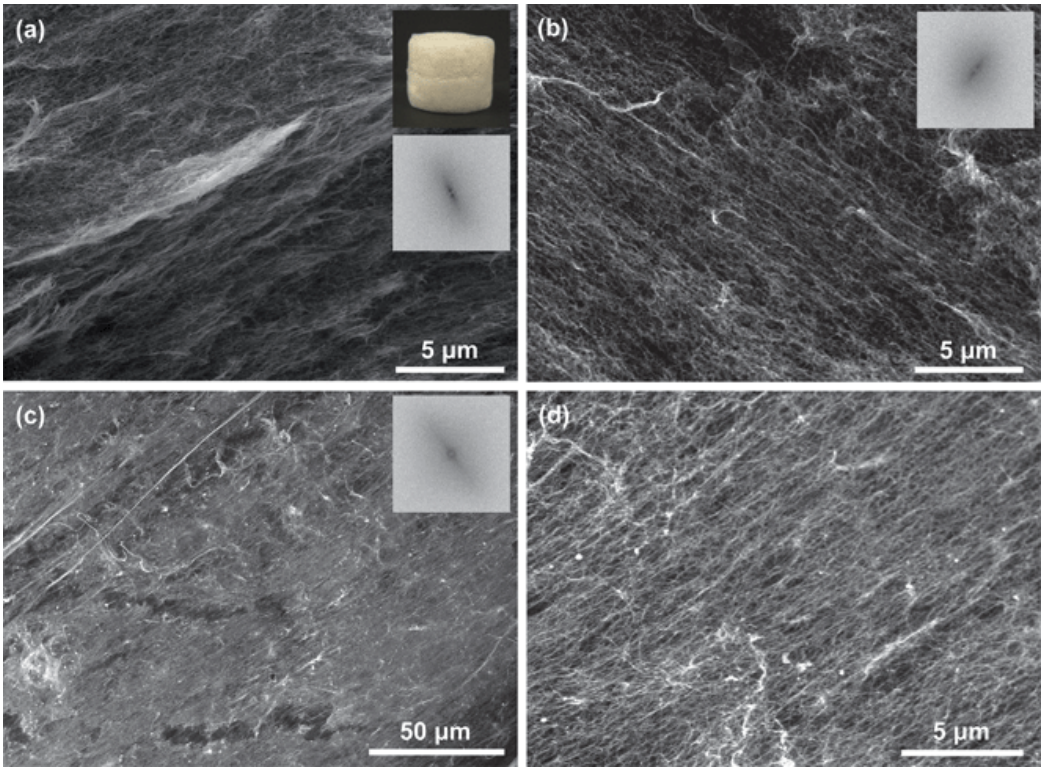

Figure 2.8: SEM of 0.4% CNF (a and b) made from wood, (c and d) from tunicate cellulose. The CNF was freeze dried after solvent exchange with tert-butyl alcohol [48].

2.7 Hydrogel activators: previous work

Gel activators trigger gelation after tunable time delay by introducing functional groups to the starting materials that activate formation of non-covalent or covalent interactions. Some common reaction mechanisms used for preparing gels using activator molecules are acid-base reactions, ion sensitive reactions, redox sensitive and binding reactions of neutral species through non-covalent reactions [54].

2.7.1 Role of gel activators

Supramolecular gelation based on low molecular weight molecules has been extensively studied [55]. In these gels, the fibrils first grow into one dimensional chains, as driven by non-covalent interactions. Gelation ensues when there is a continuous network of participating fibrils formed by self-assembly. The final mechanical properties of the obtained gels are controlled by the strength and density of the molecular interactions, depending on the self-assembly process. Figure 2.9 shows the schematics of the molecular interactions and self-assembly which leads to gelation using low molecular weight molecules.

The mechanical properties of the gels in general are governed by degree of crosslinking, mechanical properties of the participating fibrillar units forming the skeleton, distance between crosslinking points, etc [55]. It is relevant to control the crosslinking processes in order to have control over the gelation and the emerging properties. The gel activator molecules can thus become feasible where the final mechanical properties of gels could be programmed.

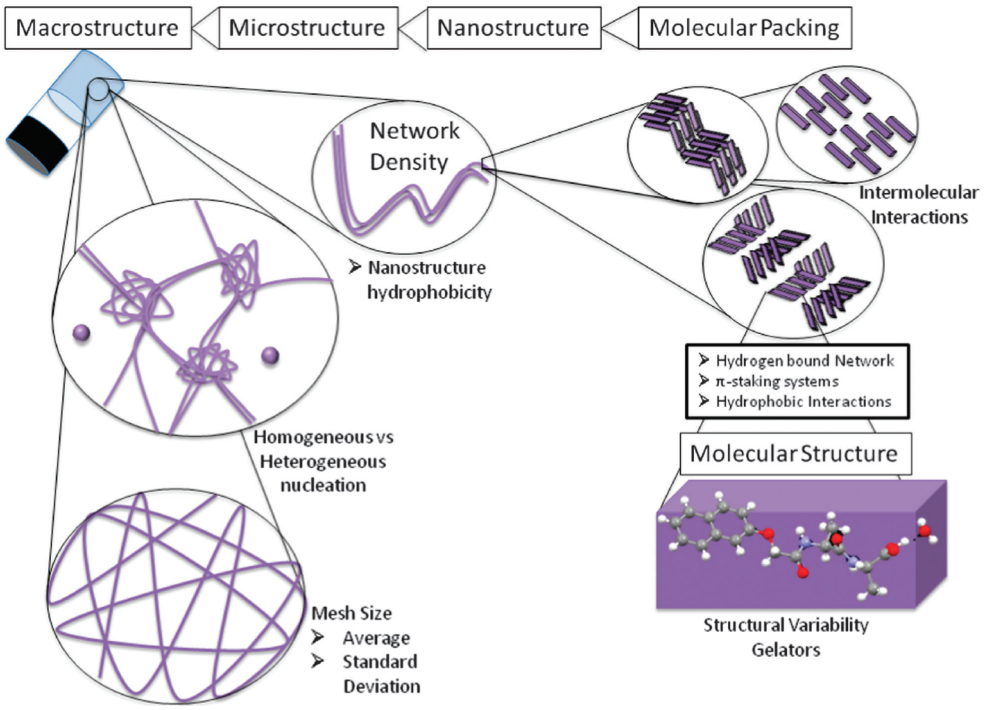

Figure 2.9: Schematics of self-assembly leading to gelation [55]

2.8 Glucono-δ-lactone as gel activator

Glucono-δ-lactone (GdL) is a carbohydrate found in many natural products such as fruits, and as gluconic acid in honey [56]. It is made by fermentation of glucose followed by crystallization of lactone [57]. GdL has several industrial uses such as in dairy industry for the cheese curd formation and in meat industry as a slow acting additive [56]. The sour taste of GdL is associated with its pH. GdL hydrolyses slowly to gluconic acid which depends on the pH of the solution, concentration and temperature [58]. The pKa of gluconic acid is 3.6 [56].

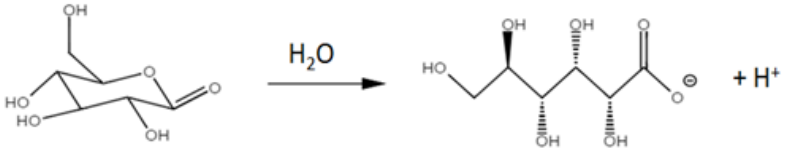

Figure 2.10: Hydrolysis of GdL.

Related to GdL-induced gelation, Dave J. Adams et al [59] first demonstrated GdL hydrolysis in producing fluorenylmethoxycarbonyl (Fmoc) dipeptide hydrogels. They form hydrogels in acidic conditions but the standard acid addition techniques lead to inhomogeneous gels. To overcome this, slow control over pH was achieved by GdL hydrolysis. An advantage of pH triggered gelation is that it allows the self-assembly process to be followed over time. Another means to control kinetics of self-assembly can be achieved by controlling the hydrolysis rate of GdL by varying the temperature [60]. Besides, the co-assembly of oppositely charged particles can be made possible by utilizing similar kinetic control of GdL hydrolysis rate [61].

Yury Shchipunov et al [62] successfully used pH triggered gelation in building hydrogels out of chitosan and clay; Figure 2.11. Here, the pH dependent charging of chitosan is achieved by GdL hydrolysis. The clay particles which are negatively charged are held towards the charged chitosan molecules by electrostatic interactions and this physical crosslinking induces gel formation.

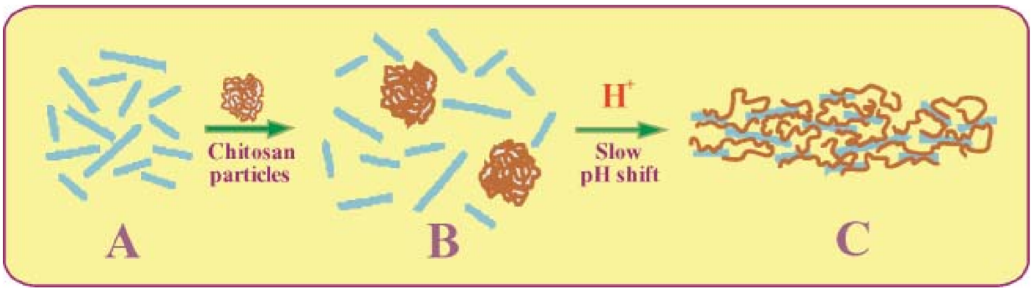

Figure 2.11: Formation of chitosan clay hydrogels by GdL hydrolysis [62].

In a recent work [63], time programming of self-assembly with a self-regulating mechanism was achieved by taking advantage of the pH trigger. Hence, it can be seen that using GdL hydrolysis to induce pH triggered reactions has more potential to form stable structures.

In this work, we explored the use of kinetic control of colloidal nanocellulose through pH to form delayed gelation. The pH rate control is controlled by the GdL hydrolysis rate. This opened up the possibility of having a chemically programmed timer.

2.9 Hydrogels and aerogels with electroactive polymers

Hydrogels with conducting polymers have been shown to find applications in robotic applications [64], making electrodes [65–69] and many other electronic applications [70–72]. An important advantage is the switching of electrical properties based on redox reactions. Hydrogels with conductive polymers based on nanocellulose materials are becoming popular due to the remarkable mechanical properties of nanocellulose and its biocompatibility [73]. Common ways of incorporating conducting polymers in the gel are by infiltration [74], electropolymerization and chemical polymerization [75, 76].

The infiltration of conductive polymers relies on the solubilities of the matrix and the electroactive material. This implies that the two components should possess similar solubility properties to yield hydrogels with optimal conductive properties. For example, CNF hydrogels had been infiltrated with few walled carbon nanotubes (FWCNT) and freeze cast to forms self-standing aerogels [77].

The electroactive hydrogels can be achieved by in-situ polymerization of monomers. The polymerization reaction is carried out either by chemically or electrochemically. An example of electropolymerization is the electrodeposition of poly(aniline) (PANI) on to CNF aerogel incorporated with silver; Figure 2.12. The disadvantage of polymerization techniques is that it is difficult to control the reaction and it is highly dependent on the environment [78] in which it is carried out.

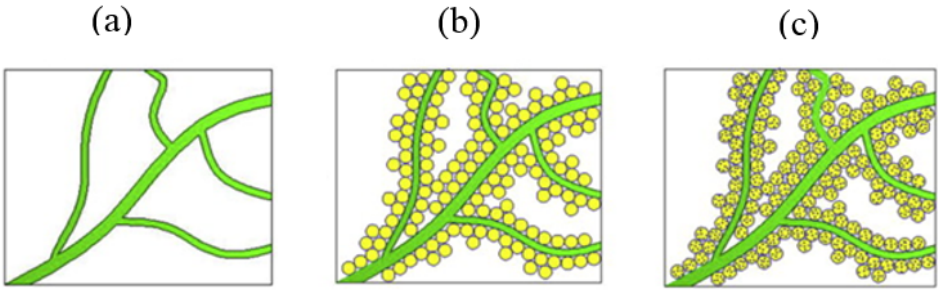

Figure 2.12: (a) CNF Aerogel (b) Ag particles were synthesized onto CNF aerogel (c) PANI was electrodeposited on to Ag/CNF aerogel [79].

In the following section, two conducting units, i.e. oligo(aniline) (TANI) and CNT, used in this work are described.

2.10 Tetra(aniline)

Tetra(aniline) (TANI) exhibits different states of conductivity and optical properties [80] by switching between different doping states by redox reactions and also by chemical doping as similarly observed in PANI [81]. Figure 2.13 shows the different doping states of TANI achieved by oxidative and acid doping. The emeraldine salt (ES) state is the conductive state which exhibits green colour whereas the emeraldine base (EB) state is a nonconducting state of purple colour. The redox doping route involves addition and removal of electrons from the nitrogen atoms of the oligomer. TANI is a potential material for building devices with switchable conductive states and also electrochromic devices.

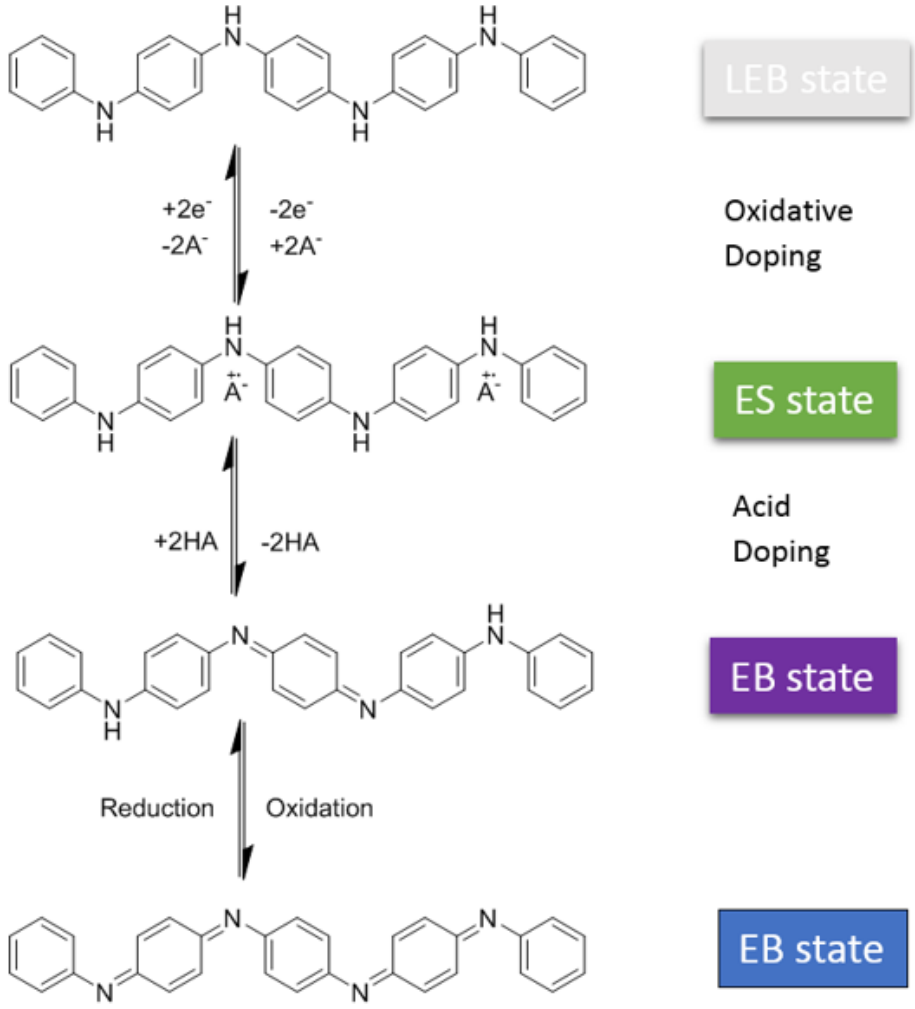

Figure 2.13: Doping of TANI to form conducting ES (Emeraldine Salt) state from LEB (Leucoemeraldine Base) state via oxidative doping and acid doping from EB (Emeraldine Base) state to ES state.

Well-defined TANI nanostructures can be produced by solvent exchange-induced self-assembly [82]. It involves the process of producing controlled aggregation and stacking of TANI molecules triggered by non-covalent interactions.This is achieved by tuning of chemical conditions between doping acid of TANI and a good solvent e.g. ethanol. The rationale behind the solvent exchange process is that when TANI gets doped by acidic conditions, the dopant anions significantly influence the interchain packing distance and thereby influence the morphology. It was observed that HCl resulted in the formation of self-assembled nanowires while acids like camphorsulfonic acid consisting of bulky anions resulted in not so well-defined structures of TANI.

The obtained nanostructures were found to contain crystals in which the crystallization process is governed by nucleation and growth by hierarchical assembly [83]. The nucleation centres dictate the growth process and the small feature sizes undergoes hierarchical assembly to merge and produce 2D nanowires or nanosheets or 3D plates with time; Figure 2.14. The crystallinity and crystal dimensionality can be controlled by controlling the solvent conditions like polarity which determines the non-covalent interactions. Thus, this hierarchical assembly paves way for producing ordered structures which shows anisotropy.

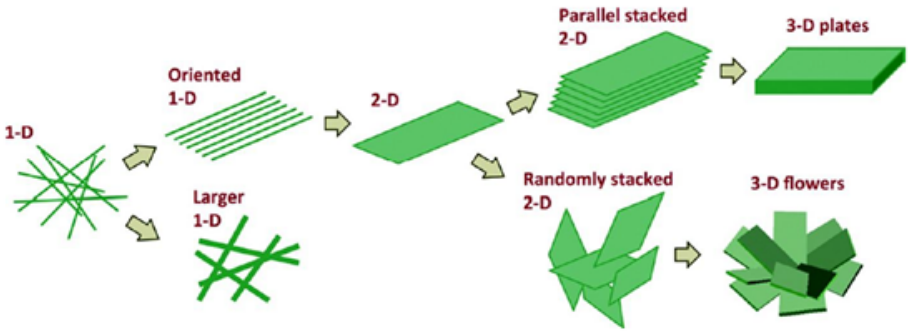

Figure 2.14: Hierarchial self-assembly of TANI crystals to form different dimensions and shapes [83].

2.11 Carbon nanotubes

Carbon nanotube (CNTs) are long cylindrical structures which can be imagined to be graphene sheets which are rolled into tubes. The structure of CNT is described by its chirality, defined by chiral angle and vector. The chiral angle quantifies the amount of twist in the tube. The electrical properties of CNT depend on the chiral angles. The zig-zag nanotubes corresponds to 0° chiral angle and armchair ones correspond to 30° chiral angle [84]; Figure 2.15. The armchair tubes denoted as (n,n) are always metallic while zigzag tubes that are (n,0) in which n is a multiple of three are metallic. All tubes that are defined by the relation $n - m = 3p \pm 1$ are semiconducting.

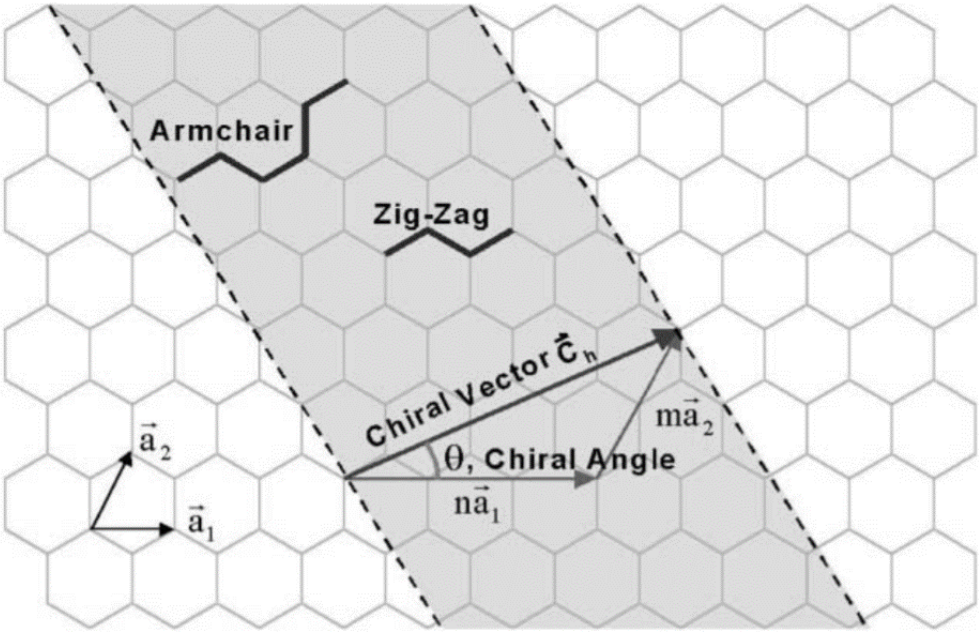

Figure 2.15: Hexagonal graphite sheet rolled into CNT showing armchair and zig-zag conditions [84].

CNTs can be classified as single walled carbon nanotubes (SWCNT), few walled carbon nanotubes (FWCNT), or multi walled carbon nanotubes (MWCNT) depending on the number of rolled layers of graphene sheets [85]. CNTs consists of both sp^2 and sp^3 hybridized carbons and the ratio of sp^2 and sp^3 hybridized atoms determines the reactivity of the CNTs. The mechanical properties of CNTs are comparable to graphene and the tensile strengths were found to be close to 63 GPa which makes them ideal composites for

making tough composite materials [86]. The effect of adding nanotubes to conducting polymers resulted in composites with higher conductivity in addition to better mechanical properties [87]. The poor solvent dispersibility of CNT makes them hard to utilize in processing of composites. Hence physical and chemical modifications are made to disperse them. A common chemical modification to improve dispersibility of CNT involves the oxidation of CNTs. This is achieved in the presence of strong acids such as sulphuric acid and nitric acid [88]. In physical methods, additives are used which provide interactions with the CNTs. For example, CNTs are dispersed using surfactants and by ionic liquids [89, 90].

Efforts have been made to combine the mechanical and electrical properties of CNTs with nanocellulose. For example, Wang et al [91] combined oxidized FWCNT with CNF by ultrasound treatment for homogenization. This is followed by freeze drying with liquid propane leading to the formation of composite aerogels which showed conductivity of the order of 10 mS/cm. Compressing the aerogel resulted reversibly increased conductivity. Thus, combining CNTs with CNF has potential for building composites with multifunctional properties.

Chapter 3

Overall aims and objectives

3.1 Chemically programmed gelation of cellulose nanofiber gels

The first aim of the present work is the following: TEMPO oxidized CNF consists of sodium carboxylate groups in the C6 position promoting dispersion in water. When GdL is added, a drop of pH over time occurs due to the GdL hydrolysis to gluconic acid. The consequent protonation of carboxylic groups on the CNF surface induces changes in the hydrophobic properties and promotes hydrogen bondings between CNFs. The hypothesized mechanism suggests that the dispersibility reduces based on the protonation extent of the fibrils; Figure 3.1. This protonation promotes the fibrillar aggregation to form network structure resulting in the formation of gels.

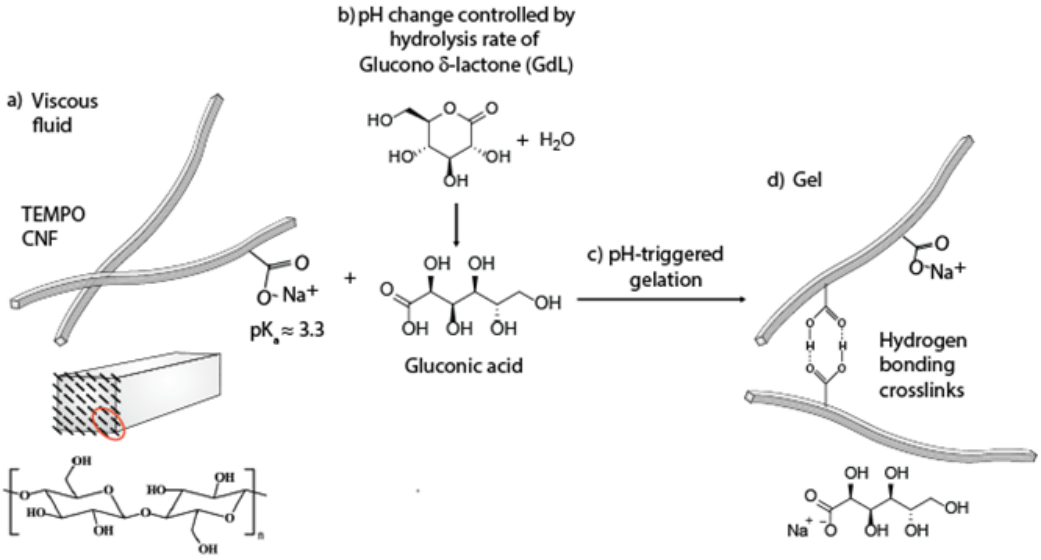

Figure 3.1: Schematics of chemically programmed colloidal gelation

3.2 Chemical programming to produce electroactive hydrogels

The second aim is to search ways to incorporate functional materials with interesting electronic and optical properties, i.e. conductive polymers and electroactive molecules, within the hydrogels.

First TANI is chosen as the material to be incorporated. TANI becomes an oligo(electrolyte) bearing a positive charge when acid-doped. It will be explored whether TEMPO-CNF/TANI hybrid hydrogel can be constructed by chemical programming by TANI doping and mutual electrostatic interaction to the anionic TEMPO-CNF by GdL slow hydrolysis to gluconic acid [92].

Hybrid hydrogels will also be studied using strong acid oxidized CNT, where the interaction to CNF is mainly driven by the hydrogen bondings.

Chapter 4

Materials and Methods

4.1 Materials

TEMPO oxidized CNF gel of 1.1 wt% was prepared from birch pulp. The obtained gel was diluted to 0.2 wt% by mixing the stock gel with Milli-Q water and subjecting it to vigorous stirring for about 24 h. This is followed by centrifugation at 8000 rpm for 20 min. The obtained dispersion is continuously stirred for about 24 h to obtain the final TEMPO-CNF dispersion. GdL, molecular weight 178.14 g/mol, was purchased from Sigma Aldrich. TANI EB, molecular weight 440.55 g/mol, was synthesized using Buchwald-Hartwig cross coupling chemistry [93] in Charl Faul Group/University of Bristol. Toluidine blue O (TB), molecular weight 305.83 g/mol, was obtained from Sigma Aldrich. The FWCNT (3 wt%) was obtained from Sigma Aldrich. The oxidation of FWCNTs was carried out in presence of strong acidic conditions as described in the procedure by Hung et al [88]. The conductive ink used in the impedance experiments was purchased from SparkFun.

4.2 Preparation of TEMPO-oxidized cellulose nanofiber hydrogels

For the preparation of CNF hydrogels, a fixed amount of gel activator, i.e. GdL, was added to TEMPO-CNF dispersions. After this, the dispersion was vortexed for about one minute. The prepared reaction mixture was poured into teflon mould; e.g. circular or rectangular shape. The here reported experimental results we produce from samples equilibrated at room conditions for 24 h prior characterization; unless stated otherwise.

Figure 4.1: Preparation of CNF gels

4.3 Preparation of electroactive hydrogels

Two sets of electroactive hydrogels, i.e. CNF/TANI and CNF/CNT were prepared. The preparation methods are illustrated in Table 4.1

Electroactive hydrogel	Preparation method
CNF/TANI	1 mL of 0.2 wt% TANI-EB stock solution in methanol is mixed with 1mL of 0.2 wt% TEMPO-CNF and 0.5 wt% of GdL were added to the mixture. The mixture is vortexed for a minute
CNF/CNT	oxidized CNT stock solution is dialysed for 24h. 1mL of obtained solution is diluted to 0.3 wt% and mixed with 0.2 wt% of TEMPO-CNF. GdL of 0.5 wt% is added to this followed by vortexing for a minute

Table 4.1: Procedure for preparation of electroactive hydrogels

The prepared hydrogels were poured into teflon moulds and equilibrated for 24h.

4.4 Rheological measurements

The rheological measurements were performed using a controlled strain rheometer (TA instruments AR2000 rheometer) using plate-and-plate geometry (diameter 20 mm steel plate, Figure 4.2). Samples were equilibrated at room conditions for 24 h prior rheological characterization.

Stress sweep measurements were carried out to determinate the linear viscoelastic region for the samples. The stress sweeps were made from 0.01 Pa to 40 Pa at an angular frequency of 1 Hz (Appendix A.1, Figure A.1).

From the stress sweep plot, 0.1 Pa was chosen as the oscillatory stress for all the gels. The frequency sweep measurements were performed in the range from 300 rad s^{-1} to 0.1 rad s^{-1}at a constant oscillatory stress of 0.1 Pa.

Figure 4.2: Plate plate geometry for rheology of gels

4.5 Vial inversion test

The time at which a CNF/GdL aqueous mixture forms a gel is first determined using the vial inversion test [94]. Representative experimental procedure for the synthesis of CNF hydrogel from a CNF suspension is given below. A microcentrifuge tube was loaded with TEMPO-CNF suspension (500 μL, 0.1 wt%) and GdL (1.25 mg), and subsequently vortexed for 1 min. The microcentrifuge tube was inverted for every 5 minutes until the

as-formed gel loses its flow, i.e. the gel suspension keeps suspended at the bottom of the container.

4.6 Preparation of TEMPO oxidized cellulose nanofiber gels at different temperatures

For preparation of CNF hydrogels at different temperatures, a fixed amount of GdL was added to TEMPO-CNF aqueous dispersion. The dispersion was placed inside an oven at required temperature until it gels. The gelation time at required temperature or the time until which the dispersion should be placed inside oven is determined by performing vial inversion tests at the desired temperature. The gels were allowed to equilibrate for 24 h before characterization.

4.7 Visible and near infrared spectroscopy

UV-Vis-NIR absorbance measurements were carried out in a Perkin Elmer Lambda 950 UV/Vis/NIR spectrometer. The reactivity of CNF, GdL, TB and TANI mixtures were monitored in-situ in quartz cuvette with 1.0 cm path length. Absorption spectra were recorded in the range of 900-200 nm. A representative example of sample preparation is described below.

Formation of cellulose nanofiber/toluidine blue complex. CNF/TB complex was prepared by mixing TB (0.3 mL, 0.001 wt%) and CNF (2.7 mL, 0.1 wt%). The reaction mixture was vortexed for one minute. An absorption spectrum was taken for the as-prepared TEMPO-CNF/TB complex prior addition of gel activator.

Addition of self-assembly activator. The as prepared TEMPO-CNF/TB complex was mixed with a fixed amount of self-assembly activator, i.e. GdL (60 mg), and vortexed for one minute. The as-prepared reaction mixture was rapidly transferred into an UVvis cuvette (≈30 sec) and the time-dependent UV-vis spectroscopic measurements were started. Absorption spectra were recorded with sequential scans for every five minutes for the first hour and then every ten minutes for a period of three hours.

A similar experimental procedure was followed for the in-situ characterization of the reactivity of CNF, GdL and OA mixtures. The gel was prepared in-situ by the experimental procedure described in section 4.3. The final vortexed solution was taken in a quartz cuvette and UV-Vis-NIR

measurements were made. The first absorbance spectrum was recorded around one min after gel preparation was performed.

4.8 Scanning electron microscopy

The morphology of hydrogels was imaged using a Zeiss sigma VP SEM. A wet gel is first slow frozen (≈ 1h) in a freezer at -20 °C. The as-frozen gel was vacuum dried to remove water solvent to form a CNF aerogel. This material is then Au sputtered (≈ 10 nm thickness layer) by using Emitech K100X sputter coater prior imaged. The as-prepared CNF/OA aerogel was imaged without Au coating.

4.9 Titration, pH and conductivity

Conductivity and pH measurements were measured using Mettler Toledo SevenExcellence pH meter with conductivity and pH probes, respectively.

The surface sodium carboxylate content from CNFs is determined following a conductometric titration procedure described elsewhere [95]. CNF aliquot (10 mL, 0.1 wt%) is reverse titrated with HCl standard solution of concentration 0.0285M. The HCl standard solution is added to CNF aliquot until the equivalence point is reached, i.e. point of inflexion of the conductivity vs. HCl volume curve (Appendix A.4, Figure A.4). The surface sodium carboxylate content was calculated from the equation [96]

$\sigma = \frac{cv}{m}$

where σ represents the surface carboxyl content, v denotes the amount of HCl in mL and c is the HCl concentration. The amount of carboxylic groups was found to be 1.07 milliequivalents per gram.

The drop in pH during GdL hydrolysis reaction and during gelation were measured against time (Appendix A.5) to understand the kinetics of the reaction. Conductivity measurements were done for understanding the change in the conductivity during the gel formation (Appendix A.6).

4.10 Fourier transform infrared spectroscopy

Infrared spectroscopy was carried out on a Nicolet 380 FTIR infrared spectrometer. Freeze-dried CNF aerogels (section 5.5) are characterised by FTIR. The total attenuated reflection was measured with 64 scans averaging and a resolution of 0.5 cm^{-1} from 400-4000 cm^{-1}.

4.11 Impedance spectroscopy

The electrical properties of hydrogels were taken using Zurich Instruments HF2IS impedance spectroscope in 4 terminal measurement setup. Impedance measurements were recorded employing a two-electrode system. Hydrogel samples were sandwiched between two Au/Ti electrodes on glass slides (75mm x 25 mm x 1mm). The measurements were repeated on fresh samples (minimum three samples) were recorded to ensure reproducibility between samples.

Diameter and thickness of analysed hydrogel samples were taken from optical microscopy images. Optical Microscopy measurements were performed with Leica 4500D optical microscope. Image digital analysis was carried out on Leica Application Suite Software.

Preparation of Au/Ti electrode. Au/Ti electrodes were made by sputtering 4 nm of Titanium on glass slides followed by sputtering 20 nm of Gold. The glass slides were cleaned, first, by sonification in an appropriate organic solvent and, second, by plasma treatment prior coating. Glass slides were sonicated (5 min) in the following organic solvents: acetone, ethanol and isopropanol. The washed glass slides were UV ozone treated for 20 minutes to remove the organic impurities and enhance hydrophilicity. The ready to use electrodes were connected to the wires with carbon conductive ink.

4.12 Cyclic voltammetry

Cyclic voltammetry experiments were carried out on a Metrohm Autolab PGSTAT302N and a conventional three-electrode system with a glassy carbon electrode (GCE, IJ Cambria Scientific Ltd, ϕ 3 mm) as working electrode, a platinum wire as auxiliary electrode and a Ag/AgCl (Metrohm, sat. KCl) as reference electrode. The in-situ electrochemical properties of CNF gels were recorded in an electrochemical sweeping range of -0.6 to 0.7 V with a scan rate of 100 mV/s for all the samples.

Chapter 5

Results and Discussion

5.1 Rheology of cellulose nanofiber gels

The gel properties and the nature of the entangled networks present can be probed by changes in viscoelastic properties using dynamic rheological measurements. The storage and loss moduli for CNF dispersion (0.1 wt%) were first explored after 24 h of addition of different levels of the GdL gel activator (0 wt%, 0.5 wt% and 5.0 wt%), see Figure 5.1. CNF dispersion without addition of GdL exhibit a viscous fluid behaviour, i.e. $G^{'} \propto \omega^{2}$, $G^{''} \propto \omega^{1}$, $G^{'} << G^{''}$. In contrast, upon including 0.5 wt% or 5.0 wt%, $G^{'}$ becomes almost independent of ω and $G^{'} >> G^{''}$ after 24 h of addition of gel activator (Appendix A.2, Figure A.2). Such a behaviour indicates elastic solid, i.e. gelation [97]. Approximately an order of magnitude higher storage modulus is observed, when the higher GdL concentrations is used. In addition, the time sweep on the gels further supported the transition to gel state from fluid state (Appendix A.3, Figure A.3). In conclusion, addition of GdL to a dilute suspension of CNF allows a transition from a viscous fluid to an elastic gel.

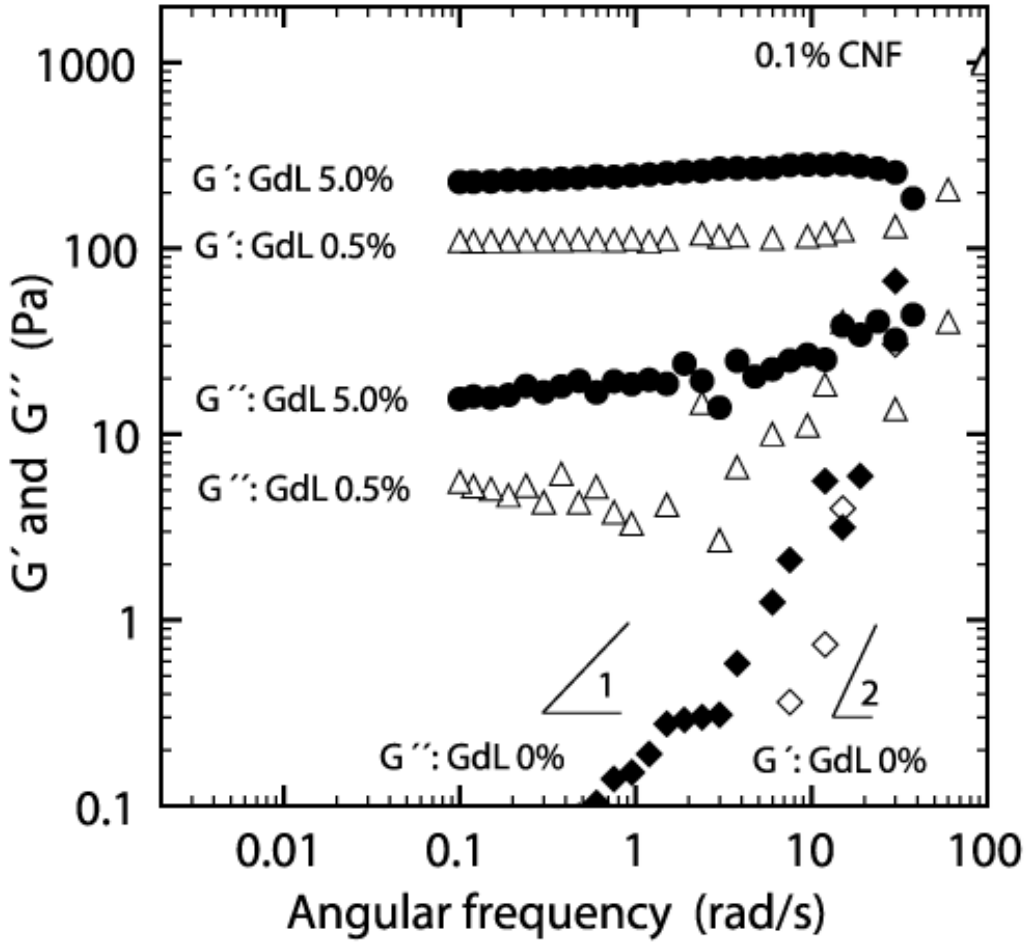

Figure 5.1: Frequency sweeps of 5% GdL, 0.5% GdL and 0.1% CNF measured at 20 °C with a constant oscillatory shear of 0.1 Pa.

5.2 Effect of the amount of glucono-δ-lactone on cellulose nanofiber gelation

CNF gels prepared from reaction mixtures with different gel activator concentrations exhibited increased storage moduli upon increasing weight fraction of GdL; Table 5.1, Figure 5.2(a). The measured data was completely reproducible and the error bars were calculated from three independent gel measurements. The ratio of storage modulus to loss modulus ($\frac{G'}{G''}$) for all the gels were in the range of 15-25 which shows relatively strong gelation.

The storage moduli vs the GdL can be associated to changes in the physical cross-link density of the three-dimensional network structure. The hydrolysis of GdL occurs at different rates depending on its starting concentration. GdL reacts with water to produce stoichiometric amounts of gluconic acid, which protonates the carboxylic salt groups in CNFs (section 2.8). This reduces the surface charge density on the CNF fibrils and allows formation of carboxylic acids which, in turn, can form hydrogen bonded dimers. Having this in mind one can think that the balance between dispersibility and precipitation of the gelator is governed by the rate at which this ongoing chemical neutralisation occurs. Hence, the key factors shaping the mechanical properties of the network like structure, i.e. degree of cross-linking, nature of crosslinking sites and microstructure, are determined by the initial concentration of gel activator.

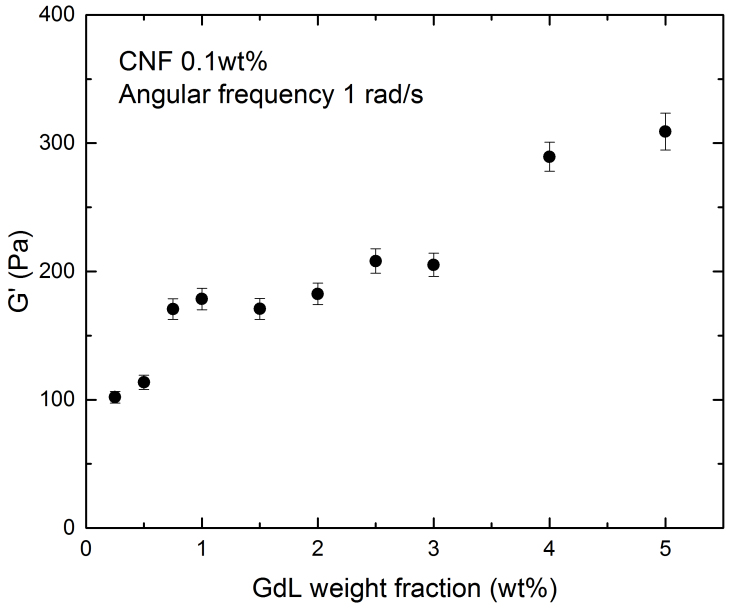

(a)

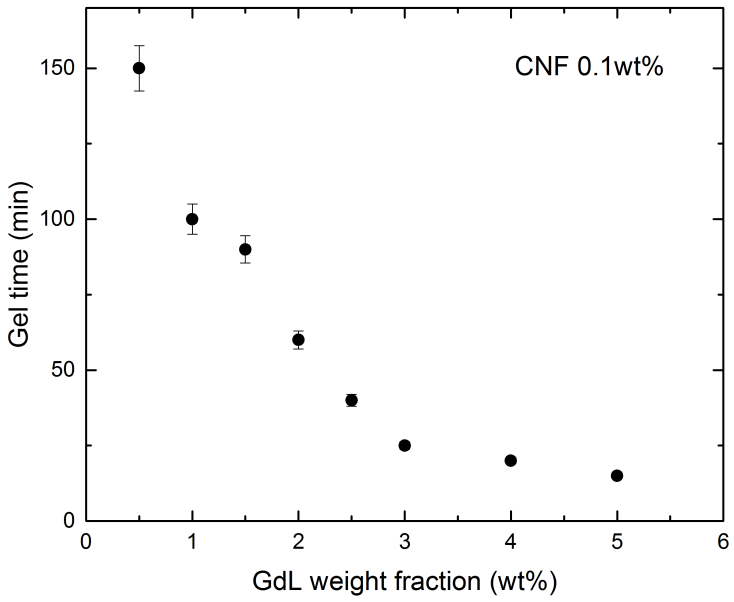

(b)

Figure 5.2: (a) Plot of GdL concentration Vs storage modulus at 1 Hz for 0.1% TEMPO-CNF gels measured at 20°C at a constant oscillatory stress of 0.1 Pa (b) Gelation Time plotted as a function of GdL concentration determined by vial inversion experiments

The synergistic effect between intermolecular hydrogen bonding interactions and hydrophobic associations produced changes on mechanical properties of CNF gels. The CNF association degree determines the strength of the network and is determined by the rate of protonation of carboxylic acids.

The mechanical properties of the CNF gels show three distinct regimes; Figure 5.2(a). For $\leq 1\%$ of gel activator, one can observe a linear increase in $G^{'}$ as a fuction of concentration of gel activator. This behaviour can be attributed to the initiation of networks as explained earlier. Between 1% and 3% of gel activator, a plateau in modulus is observed. Above 3% of gel activator concentration, one can see a linear increase of $G^{'}$. This behaviour can be attributed to new hydrophobic interactions introduced by excess gluconic acid.

Table 5.1 shows also the gelation times, determined using the vial inversion tests. In fact, in rheology the gelation time is defined as the time at which the storage modulus $G^{'}$ vs frequency crosses with loss modulus $G^{''}$ vs frequency [98]. The gelling behaviour of CNF is strongly dependent on the pH [99]. In the present case, the gelation at the highest GdL fraction was so rapid that the rheological determination of the gelation time was not possible, taken the time of the rheological measurement. Hence, the gelation times of the gels with different concentrations of GdL were measured by performing vial inversion tests (Figure 5.2(b)). The observed gelation times become shorter when the concentration of GdL is increased. This shows that the gelation times can be controlled in the range of hours to seconds depending on the concentration of GdL added initially.

GdL(wt%)	$G^{'}$(Pa)	Gel time (minutes)
0.5	113.53	150
1	178.53	100
1.5	170.8	90
2	182.53	60
2.5	208.1	40
3	205.2	25
4	289.4	20
5	309	15

Table 5.1: Mechanical and gelation properties of CNF gels precipitated from 0.1% TEMPO-CNF. Elastic modulus measured for gels measured at 1 Hz, constant oscillatory stress of 0.1 Pa and 20 °C. Gelation Gel time determined by vial inversion experiments.

We next explored whether the chemical programming by adding GdL (and its slow conversion to gluconic acid) leads to different gel properties than the direct addition of gluconic acid. Therefore gluconic acid was added drop-wise onto the TEMPO CNF dispersion, corresponding to 2% of GdL. The dispersion was subjected to vortexing for a minute and the vial inversion test indicated that the CNF gel forms almost instantaneously after mixing. The rheological measurements were performed after 24 h. The frequency sweep revealed that the mechanical properties of gels that are chemically programmed by GdL exhibited higher modulus than that of the gels prepared directly with gluconic acid; Figure 5.3. Moreover, the gluconic acid gels were quite fragile and difficult to handle when compared to the chemically programmed gels. The observed mechanical behaviour indicates that the self-assembly driven by controlled hydrolysis of GdL is a key factor for obtaining gels with better handleability and mechanical properties.

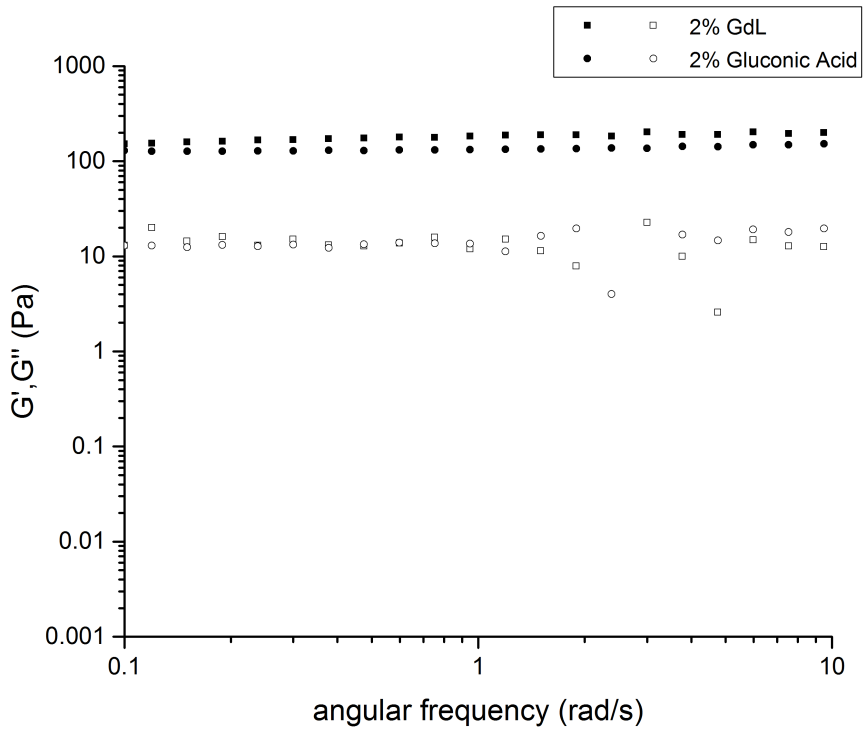

Figure 5.3: Frequency sweeps of 2% Gluconic Acid and 2% GdL recorded at 20°C at a constant oscillatory stress of 0.1 Pa.

5.3 Effect of cellulose nanofiber concentration

The effect of CNF concentration on the mechanical properties of the gels were measured by frequency sweeps using two CNF concentrations, i.e. 0.1% and 0.2%. The gels with higher CNF content exhibited considerably higher storage moduli; Figure 5.4. This can be attributed to larger number of crosslinks between CNFs, resulting in stronger network like structures. The storage modulus exhibited by 0.2% TEMPO-CNF and 3% GdL was found to close to modulus exhibited by TEMPO-CNF hydrogels prepared using HCl [48].

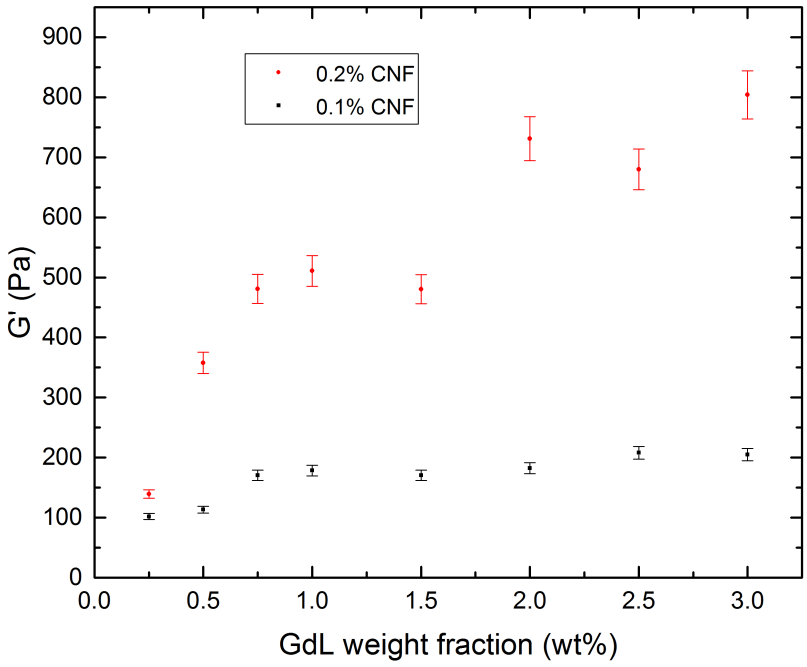

Figure 5.4: Comparison of 0.1% and 0.2% TEMPO-CNF concentration. The storage modulus at 1 Hz from frequency sweep was plotted against different GdL concentrations.

5.4 Effect of temperature on cellulose nanofiber gels

The effect of temperature on the gels was studied, as explained in section 4.6. The gelation time becomes shortened at higher temperatures; Table 5.2. This is attributed to the temperature-dependent hydrolysis of GdL which increases with increase in temperature [100]. Therefore, temperature-driven GdL hydrolysis leads to increase of probability of crosslinking between the CNFs resulting in lower gelation time.

Temperature(°C)	Gelation Time(minutes)
20	60
50	25
60	20

Table 5.2: Effect of temperature on 0.1% TEMPO-CNF and 1.5wt% of GdL

There is an enhancement of storage modulus when the temperature is increased; Figure 5.5. This results in the increase of cross-linking densities of the hydrogels which affects the mesh size of the gels [101]. The observed increase in mechanical properties may be ascribed to the increase of crosslinking densities due to temperature [102].

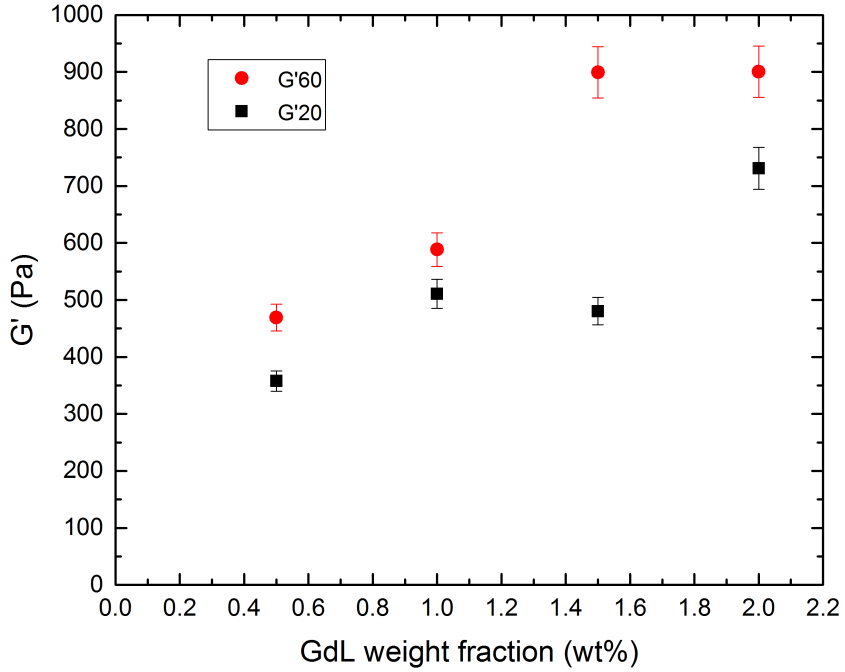

Figure 5.5: Storage modulus of CNF gels prepared in the presence of gel activator at different room temperatures: 20 and 60°C. CNF gels were prepared from 0.2% colloidal suspensions in the presence of different GdL concentrations: 0.5, 1.0, 1.5 and 2.0%. The rheological measurements were made after keeping the gels at corresponding temperatures in oven until it gelates and then equilibrating for 24 hours at 20°C.

5.5 Determination of degree of protonation of the gels

The degree of protonation of the carboxyl groups in the gels can be characterized by FTIR. Figure 5.6 shows the FTIR of TEMPO-CNF aerogels produced by freeze drying of CNF hydrogels prepared with different gel activator concentrations. The C=O carbonyl stretch of carboxylic acid groups can be identified between wavenumbers 1690 and 1750 cm^{-1}.

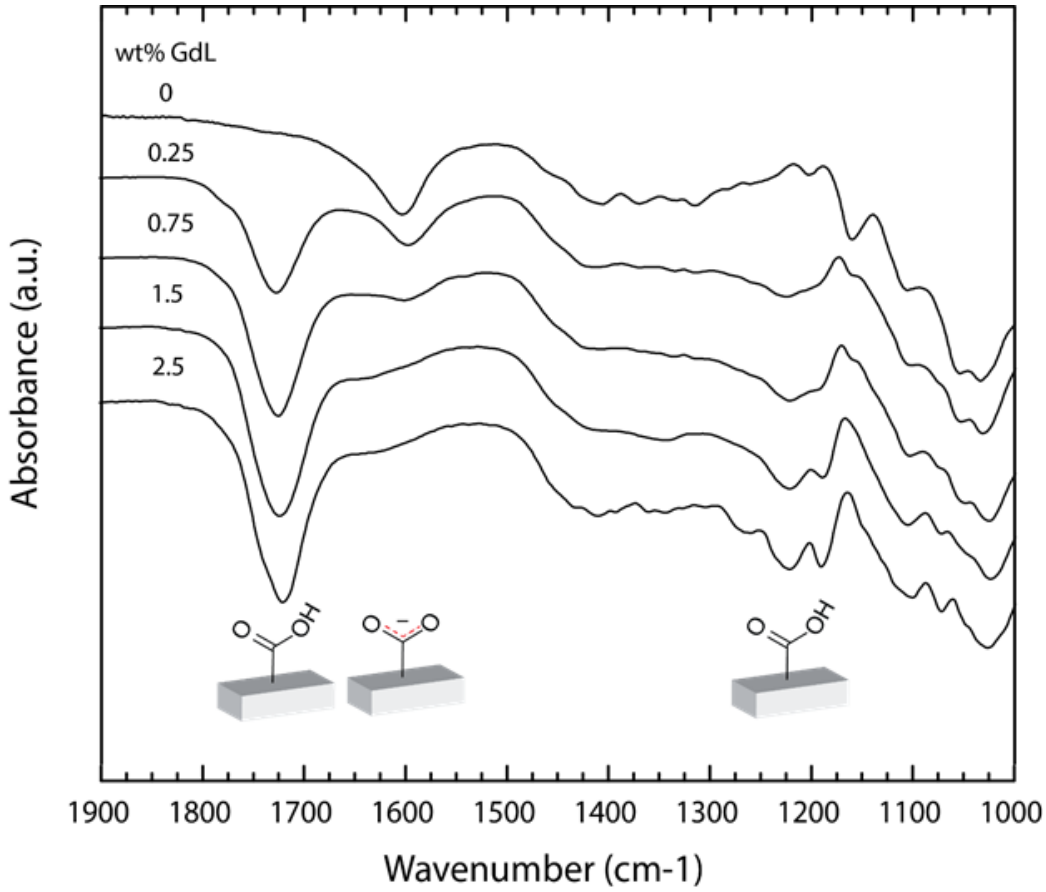

Figure 5.6: FTIR for different GdL concentrations of 0.1% TEMPO-CNF. The as-formed TEMPO-CNF gels were kept in freezer at -20°C. The frozen gels were subjected to vacuum drying to form aerogels and subjected to FTIR characterization.

From Figure 5.6, it can be observed that the changes in the carbonyl stretch can be attributed to the protonation of CNF. For 0.1% TEMPO-CNF

dispersion the peak observed around 1602 cm^{-1} indicates the presence of carboxylic group existing as $COO^{-}Na^{+}$ [96]. In the case of 0.25 wt% GdL, the peak observed at 1728 cm^{-1} shows that the carboxyl groups become protonated and a shoulder peak at 1602 cm^{-1} indicates that still some of them exists as $COO^{-}Na^{+}$. For 0.75 wt% GdL, the intensity at 1728 cm^{-1} intensifies and the shoulder at 1602 cm^{-1} starts to diminish. The shoulder observed around 1602 cm^{-1} is due to the C=O shift to lower energy. At a concentration of 1.5 wt% of GdL, it is evident from the FTIR that the peak corresponding to $COO^{-}Na^{+}$ vanishes and the peak around 1728 cm^{-1} shows a further increase in intensity. This can be inferred that at this concentration the TEMPO-CNFs are completely protonated. The broadening of peaks observed around 3300 cm^{-1} shows that the hydrogen bonding interactions increases as the concentration of gel activator is increased; Figure 5.7. This can be attributed to the larger degree of hydrogen bonding interactions between the CNF fibrils [103].

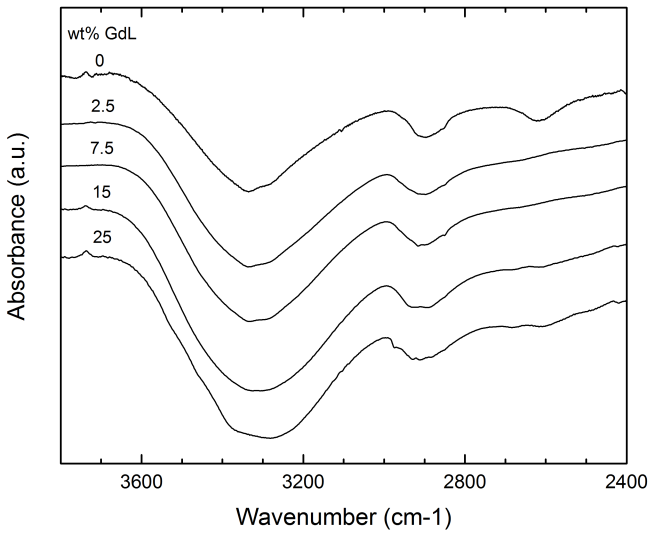

Figure 5.7: FTIR indicating the broadening of O-H stretch due to hydrogen bonding.

5.6 Protonation of carboxyl groups and its effect on mechanical properties

The degree of protonation observed with respect to GdL concentration in the FTIR has close correspondence to the observed mechanical properties of the gels. From Figure 5.2(a) and the ensuing discussion on section 5.2, it can be seen that till concentration of 1 wt% of GdL, there was a linear increase in storage modulus with increasing concentration. This is a direct consequence of increase in protonation of carboxyl groups with increase in GdL concentration. A small increase in storage modulus with increasing concentration behaviour was observed with concentrations between 1 wt% and 3 wt%. This can be attributed to the effect of protonation and interactions between gluconic acid and formed molecular gel like network. An increase in storage modulus with concentration was observed for concentrations above 3 wt%. This can be attributed to the effect coming from the excess gluconic acid which interacts effects with the completely protonated network. The interactions also increase on further increasing the concentration of GdL.

5.7 UV spectroscopy for monitoring of cellulose surface interactions

The interaction between negatively charged cellulose surfaces and cationic dye was monitored by UV-Vis-NIR. The cationic dye used in this work is toluidine blue (TB) which is used as a biological staining agent for the cells [104]. CNFs were coated with TB by simple mixing of both components. The interaction of TB molecules with negative charged surfaces produces a characteristic shift in wavelength depending on its aggregation and interaction properties, the so-called metachromasia [105]. TB molecules forms different kinds of aggregates depending on the concentration [106]. The mechanism behind aggregation is the formation of a new intermolecular bond between adjacent dyes [107].

The UV-Vis-NIR of TB molecules in water showed two peaks: one at 640 nm and the other at 600 nm; Figure 5.8(a). The peaks correspond to intermediate aggregation forms of TB molecules which depends on concentration [106]. Figure 5.8(b) shows the spectra of hydrolysis of GdL after 24 hours. The spectra do not contain any new peaks indicating that the observed TB peaks are independent of change of pH.

The UV-Vis-NIR spectra showed three distinct peaks for the system

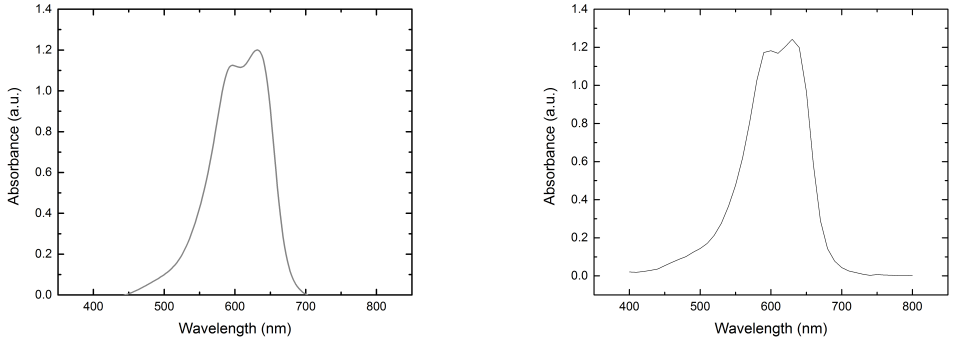

(a) (b)

Figure 5.8: (a) UV-Vis spectra of aqueous solution of TB (0.001%) (b) after 24 h of reaction with GdL of 2% GdL

with TB and TEMPO-CNF. A peak at 540 nm which corresponds to the aggregation of TB molecules due to electrostatic interactions between cationic TB molecules and anionic TEMPO-CNF fibrils. The peak is attributed to the polymeric structure of dye molecules and the formation of vertical stacking of dyes called as H-aggregates [105, 106]. A second peak was observed around 595 nm and a third at 640 nm which corresponds to intermediate aggregate forms of TB molecules [108]. As time proceeds, the peak corresponding to electrostatic interactions starts to decrease and the peaks corresponding to intermediate aggregations increases. This behaviour is depicted in Figure 5.9(c).

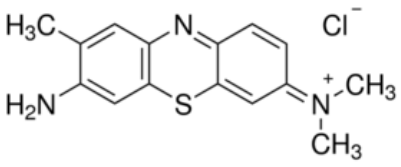

(a)

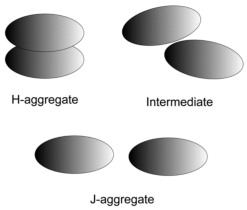

(b)

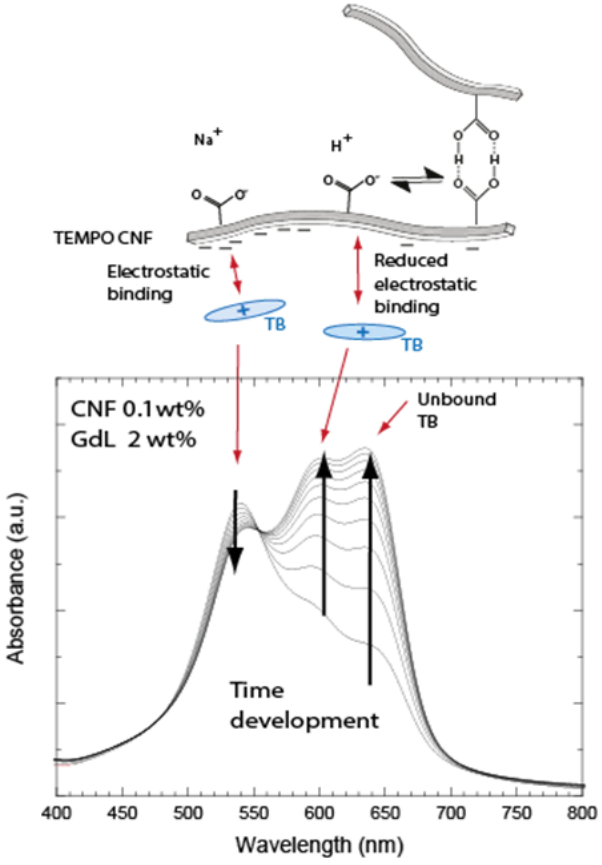

(c)

(d)

Figure 5.9: (a) Structure of TB. (b) Different aggregates of TB [106] (c) The spectra show electrostatic interactions of TB with TEMPO-CNF and GdL at different times. The rationale behind the electrostatic interactions are depicted in the scheme. (d) Observed colour transition after gelation. Lavendar colour indicates colloidal suspension and blue colour indicates the gel. The spectra were recorded with 0.1% TEMPO-CNF, 2% GdL and 0.001% TB

The peaks observed around 540, 640 and 600 nm were plotted against time to evaluate the changes in intermolecular interactions that occurs during gelation. To describe this, two cases were taken: fully and partially protonated CNF confirmed by FTIR measurements (section 5.5). The cases were taken to evaluate the effect of protonation on the observed behaviour.

The observed change of intensity ratios for the peaks is produced by the changes in the electrostatic binding between CNFs and TB molecules as the protonation proceeds along time. As soon as the GdL hydrolysis starts to supply H^+ ions, the TEMPO-CNFs start to protonate. The protonation of TEMPO-CNFs gives rise to new hydrophobic interactions between them. These interactions disrupt the stacking of TB molecules over the CNFs along time.

For samples prepared above 1.5 wt% GdL (Figure 5.10(a)), the intensities observed after the gelation time showed that the peaks caused by intermediate aggregates is greater than the electrostatic binding interactions between CNF fibrils and TB molecules. This is attributed to the full protonation of the carboxylic groups in the CNF leading to less bound TB molecules. In contrast for samples prepared with less than 1.5 wt% of GdL (Figure 5.10(b)), the final intensities indicated that the electrostatic binding interactions are greater than the intermediate aggregates. The observed behaviour is in validation with the presence of unprotonated carboxylic groups. Hence this method shows a way of monitoring binding interactions along time.

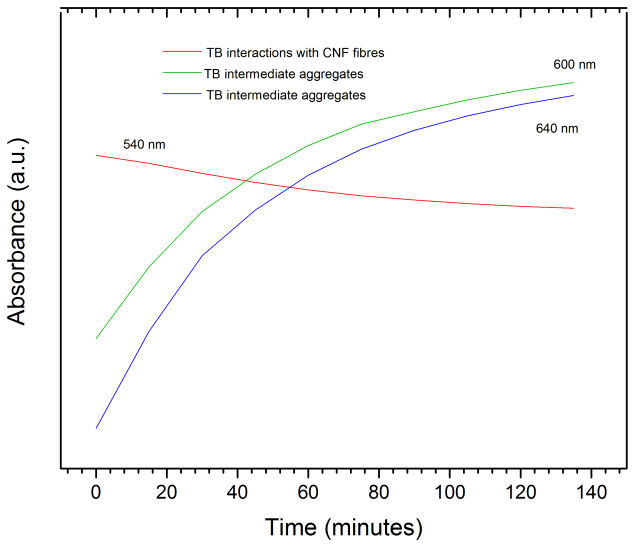

(a)

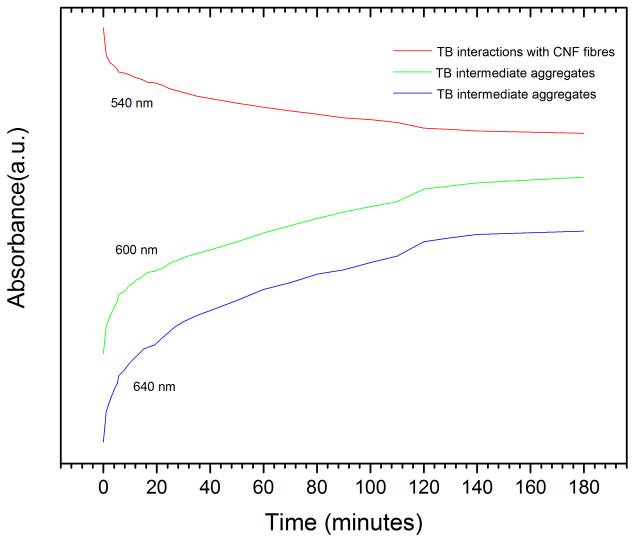

(b)

Figure 5.10: Measured UV absorbance for peaks observed at 540, 600 and 640 nm along the chemically programmed gel formation process. (a) 0.1% TEMPO-CNF 2% GdL. (b) 0.1% TEMPO-CNF 0.5% GdL.

In the case of fully protonated CNF, the time at which the electrostatic binding peaks crosses with intermediate aggregate peaks gives an approximate gelation time. The observed gelation times using UV-Vis-NIR was found to be close to the gelation times determined using vial inversion tests; Figure 5.11.

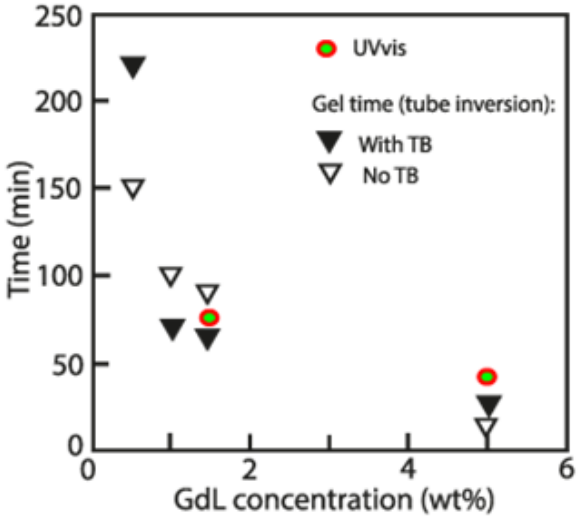

Figure 5.11: Comparison of gelation times determined using vial inversion and UV-Vis-NIR. Vial inversion tests were carried out using a 500 μL solution in a microcentrifuge tube.

TEM characterization was made to confirm the coating of CNF fibrils with TB molecules after 24h of stabilization. The TEM shows TB aggregates with CNF fibrils (Appendix A.11, Figure A.11), but it is hard to confirm if the CNFs are getting coated with TB.

5.8 Chemical programming of cellulose nanofiber-based gels with electroactive properties

The GdL hydrolysis-driven gel formation produces CNF networks with tunable molecular interactions, i.e. hydrophobic and hydrogen bonding interactions. Moreover, the dynamic kinetic control over surface molecular interactions of CNFs unlocks the possibility of controlling molecular associations between different components. Here we study the GdL hydrolysis-driven hybrid gel formation consisting of different components.

5.8.1 Monitoring of assembly of tetra(aniline)-cellulose nanofiber system

To make conducting hydrogels based on CNF/TANI mixtures, it becomes necessary to control the pH to tune the electrostatic interactions, as a sudden drop of pH would lead to phase segregation. In acidic conditions, TANI is known to precipitate resulting in the formation of anisotropic structures[109]. The observed anisotropic structures are a result of a combination of hydrogen bonding and electrostatic interactions (section 2.10). GdL hydrolysis reaction produces pH rate control which could enable control over the intermolecular interactions between positively charged TANI molecules. This also lead to the thought, whether the method enables the possibility to produce coating of positively TANI molecules over negatively charged CNF fibrils driven by chemically programmed electrostatic interactions.

To achieve such a coating, the concentration of GdL was chosen such that the hydrolysis rate does not induce precipitation of TANI. TANI hydrogels produced by different hydrolysis rates were analysed using SEM. The experiment conducted with fast hydrolysis rate resulted in phase segregation which is confirmed by presence of crystals of TANI under SEM (Appendix A.8, Figure A.8). Hydrogels formed with slow hydrolysis rate of GdL exhibit no phase segregation (Appendix A.9, Figure A.9). The observed material structure can be attributed to slow formation of cationic TANI species without precipitation which interact with anionic TEMPO-CNF to form electrostatic assembly. The presence of anionic binding sites on CNF can be ensured by the use of initial GdL concentrations below 1.0 wt%.

5.8.2 Acid doping properties of tetra(aniline) hydrogels

The as-prepared TANI hydrogel retains its acid doping properties. A TANI ES film was prepared by complete evaporation of water at room temperature. The film was exposed to concentrated ammonium hydroxide vapours. UV-Vis was taken for the TANI ES film exhibited characteristic peaks around 440 and 800 nm; Figure 5.12. The film exposed to base exhibited a peak around 600 nm and no presence of doping peaks. This switch of properties is an indication that the CNF does not affect the acid doping properties of TANI.

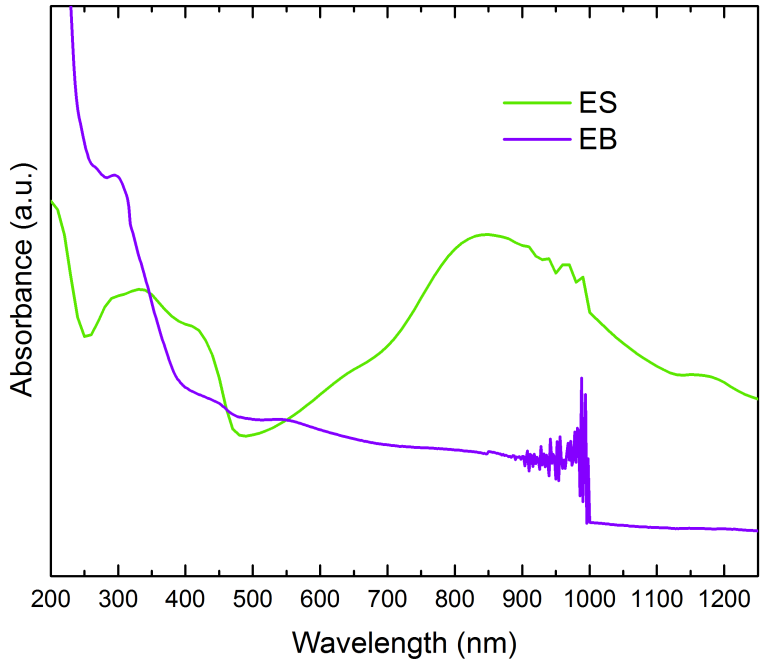

Figure 5.12: EB and ES states in the UV-Vis-NIR. The spectrum was taken for the prepared TANI hydrogel indicated as ES. The hydrogel was then made into a film by room temperature evaporation of water. The prepared film was then exposed to ammonium hydroxide vapours and spectrum was taken, indicated as EB. The artifact observed in the EB plot is due to the lamp change in the spectrometer which happens between 900 and 1000 nm.

5.8.3 Mechanism of cellulose nanofiber-tetra(aniline) hybrid gels

The possible mechanism for the formation of gels with TANI is illustrated in Figure 5.13. Initially, GdL hydrolysis product, i.e. gluconic acid, protonates TANI to form charged doped species [83]. This doping process occurs in competition to the protonation-driven gelation process undergone by CNF. The gelation process continues whilst cationic TANI species interacts electrostatically with anionically charged CNF fibrils.

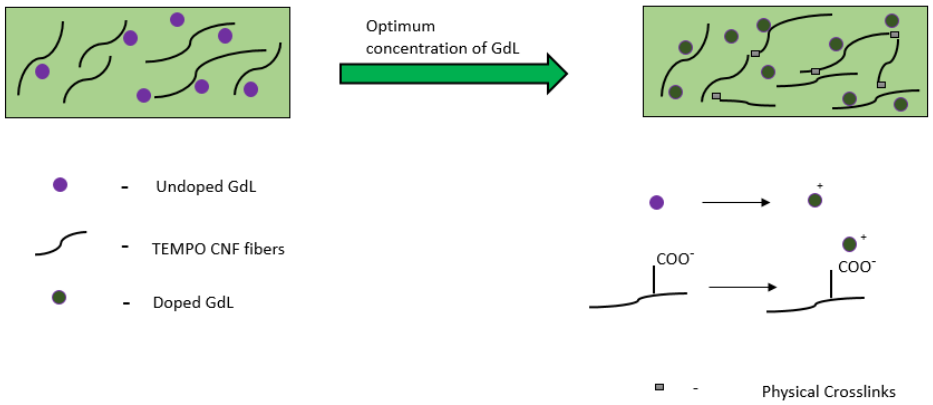

Figure 5.13: Scheme for coating of TANI over CNF fibres. Doping of TANI occurs first due to pKa which makes them positively charged and is held to negatively charged CNF fibers due to electrostatic interactions.

The acid doping process of TANI in presence of CNF was followed by UV-Vis spectroscopy; Figure 5.14. It revealed peaks around 300 nm, 440 nm, 600 nm, 800 nm and 1150 nm during the initial stages of the reaction. The peaks close to 440 nm and above 800 nm are associated to acid doping of TANI [110]. The peaks observed close to 600 nm is due to presence of TANI in EB state [83]. The presence of peaks associated to both doped and undoped peaks may be explained by the presence of different cationic TANI species. Although, there is no clear explanation for the stabilization of TANI species under the performed experimental conditions. A possible explanation may be the presence of gluconic acid influencing the solubility of protonation driven TANI species.

As the hydrogel formation proceeds with time, the doping peaks start to increase while the undoping peak decreases. The intermediate states of doping may be confirmed by the presence of doping and undoping peaks

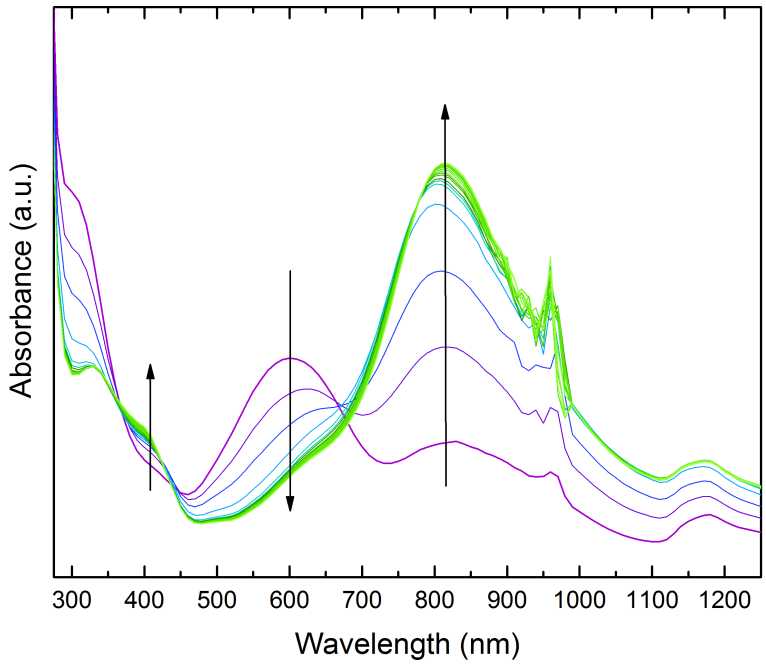

Figure 5.14: UV-Vis-NIR spectra of the acid doping process of TANI inside the hydrogel. The spectra were taken at every two minutes. The purple colour inidicates the initial EB state and the green colour spectra indicates the transformed ES state. The artifact observed in the EB plot is due to the lamp change in the spectrometer which happens between 900 and 1000 nm.

during the early stages of the reaction. This gives an indication that the doping process of TANI inside the hydrogel can be controlled. After the gel was completely formed, the UV-Vis confirmed the complete acid doping of TANI (green colour hydrogel).

Hence, one can conclude that the aforementioned method is an in-situ bottom up approach for producing electroactive hydrogels.

The preparation method discussed has potential for producing gels in which the interaction between CNF and the conducting polymer is dominated by different intermolecular interactions. For example, the dominant interaction in CNT hydrogels is hydrogen bonding interactions; Figure 5.15(a). The method also enabled incorporation of conducting polymers with intrinsic charge such as poly(3,4-ethylenedioxythiophene) polystyrene sulfonate (PEDOT: PSS); Figure 5.15(b). In addition to this,

the method enabled production of stacked gels consisting of a CNF hydrogel stacked over a TANI hydrogel; Figure 5.15(c).

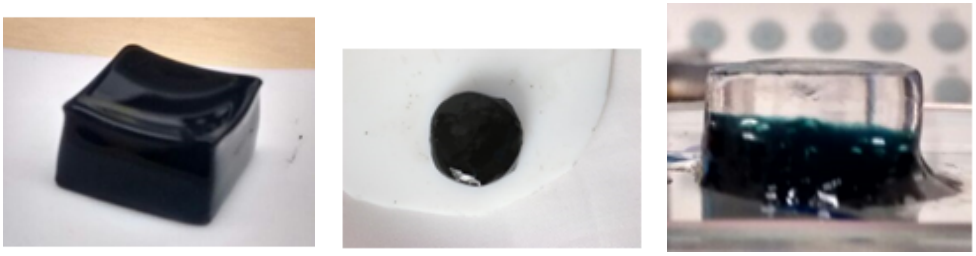

(a) (b) (c)

Figure 5.15: Photographs of different electroactive hydrogels. (a) CNT hydrogel (b) PEDOT: PSS hydrogel (c) stacked gels

5.9 Electrical properties of hydrogels

Impedance spectroscopy was used to measure the electrical properties of conductive hydrogels. EIS analyser was used for fitting the obtained impedance spectra. Randles circuit was used as the equivalent circuit model for characterizing the electrical properties of the gels [111]. Figure 5.16 shows the randles circuit. The randles circuit consists of series bulk resistance (R1), a constant phase element (CPE1) for the double layer capacitance, a Warburg element (W1) for the diffusion and a charge transfer resistance (R2). W1 was replaced by CPE at low frequencies as it resulted in a better fit.

Figure 5.16: Randles Circuit. R1-series bulk resistance, R2-charge transfer resistance, CPE1- constant phase element, W1-warburg element.

The series resistance value was then converted to ionic conductivity by using the formula [112]:

$\sigma = \frac{t}{R.A}$

where σ is the ionic conductivity, R is the bulk resistance to ions flow, t is the thickness of the gel that is in contact with the electrodes, A is the area of the gel in contact with electrodes.

5.9.1 Effect of cellulose nanofiber concentration

The ionic conductivity of gels with different TEMPO-CNF concentrations were measured; Figure 5.17. For all the measured samples, the impedance spectra showed a semicircle at high frequency region and an inclined straight line at lower frequencies. The small diameter of semicircle indicates that the charge transfer resistance is low in the gels [75].

The results indicate that on increasing the CNF concentration the ionic conductivity decreases; Table 5.3.

The observed results can be attributed to the conduction mechanism in the hydrogels. In hydrogen bonded systems, the conduction of protons occurs by a process called as Grotthus mechanism [113]. In this mechanism, the

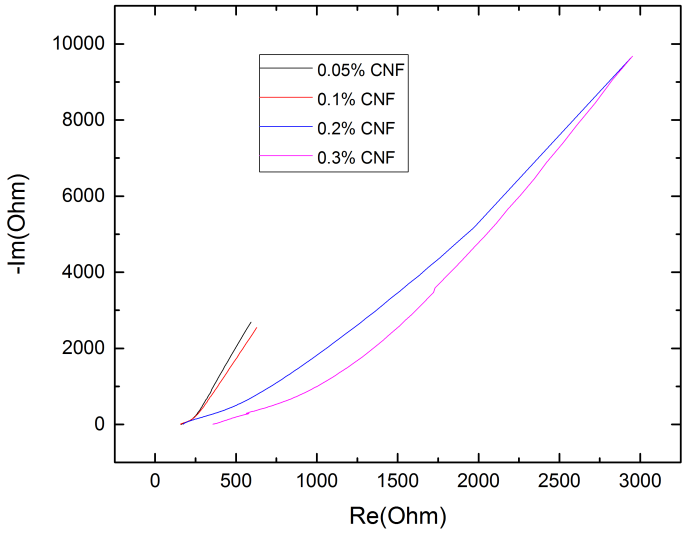

Figure 5.17: Impedance Spectra of hydrogels with different TEMPO-CNF concentrations. Samples were gelated with 2% GdL

CNF(wt%)	Ionic Conductivity(mS/cm)
0.05	0.16
0.1	0.17
0.2	0.144
0.3	0.082

Table 5.3: Results of fitting impedance spectra using Randles circuit where Warburg is replaced by CPE

protons get diffused through the network by successive hopping along bonds with neighbouring chains. This mechanism of transport of ions is opposed by the segmental motion of the polymer chains resulting in the reduction of conductivity as the concentration of CNF is increased. A similar behaviour was observed for blend gel electrolytes consisting of poly(vinyl alcohol) and poly(acrylic acid) [114]. Table 5.3 shows the results of obtained conductivities for different CNF concentrations.

5.9.2 Effect of glucono-δ-lactone concentration

The electrical properties of gels prepared with different GdL concentrations were measured with impedance spectroscopy. The spectra showed a semicircle at high frequency region and a straight line at lower frequencies (Figure 5.18). The results indicated that the value of ionic conductivity increases as the concentration of GdL was increased. Table 5.4 shows the results of the obtained conductivity.

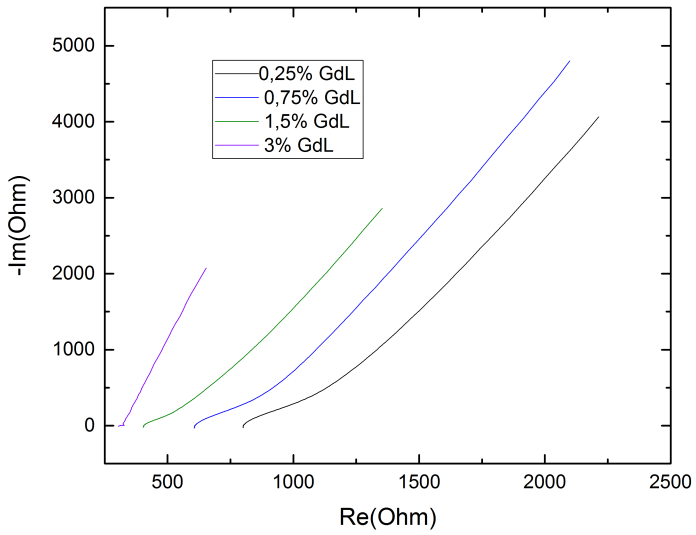

Figure 5.18: Impedance spectra of gels for different GdL concentrations

For increased concentration of GdL, the ionic conductivity values increased. This may be attributed to the increase of free gluconic species inside the gels produced.

CNF($wt\%$)	Ionic Conductivity(mS/cm)
0.25	0.0954
0.75	0.126
1.5	0.191
3.0	0.252

Table 5.4: Results of fitting impedance spectra using Randles circuit where Warburg is replaced by CPE

5.10 Electroactive hydrogels

Electroactive hydrogels were prepared with TANI and CNTs. Hydrogels with concentration of 0.4 wt% CNT was analysed using impedance spectroscopy. The CNT gels showed enhanced ionic conductivity in the perpendicular direction than in parallel direction which means that the material shows anisotropy.

Hydrogels of TANI were prepared with 0.05 wt% of TANI and electrical measurements were performed on the gels. The TANI gels showed conductivity of 0.038 mS/cm in both directions indicating no anisotropy. The reason for the non-observance of anisotropy is unknown and need to be further studied for drawing conclusions. The results obtained were summarized in Table 5.5.

Material	Conductivity(mS/cm)	Circuit
TANI	0.0038	Randle's Warburg impedance replaced by CPE at low frequencies
FWCNT	0.8 in parallel direction and 2.3 in perpendicular direction	Randles circuit

Table 5.5: Conductive properties of TANI and FWCNT gels

The addition of electroactive materials to CNF hydrogels introduces differences in the conductivity. Hydrogels without electroactive materials showed conductivity of 0.091 mS/cm. CNT and TANI hydrogels exhibited conductivities of 2.3 and 0.038 mS/cm respectively. Clearly there is an enhanced conductivity for the CNT case although lower conductivity values were recorded for TANI gels.

5.11 Electrochemical studies on hydrogels

The electrochemical studies of CNF and CNF/TANI hydrogels were made using cyclic voltammetry. The CV of 0.2 wt% CNF hydrogels prepared with 0.5 wt% GdL is shown in Figure 5.19.

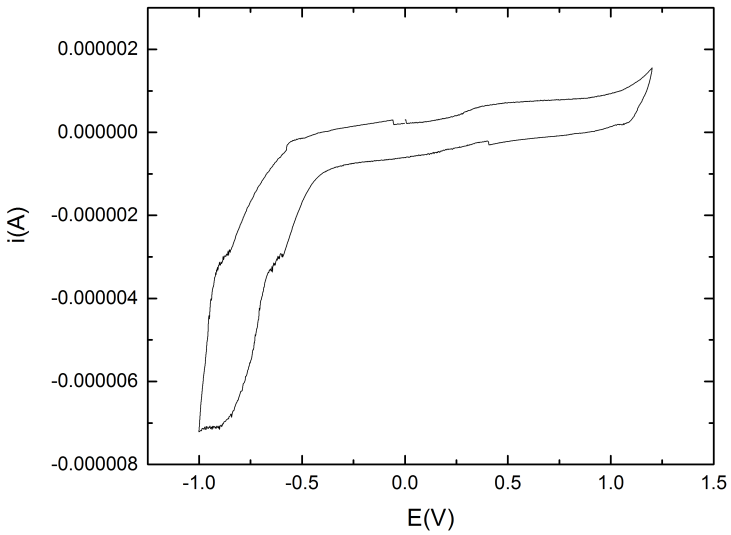

Figure 5.19: CV of 0.2% CNF and 0.5% GdL. Scan rate 100 mV/s.

The result showed no distinct peaks in the CV indicating that no redox reactions are occurring in the CNF hydrogels. For the case of CNF/TANI hydrogels, the gels were prepared such that the ratio of CNF to TANI is 3:1. Three cycles of CV were performed (Figure 5.20) with the voltage range and scan rate specified in section 4.12.

On comparing with CNF hydrogels, the TANI hydrogels showed distinct peaks around 0.43 V and 0.25 V in the CV which can be ascribed to the occurrence of oxidation and reduction reactions in the hydrogel which needs to be characterized further in order to derive conclusions. These results indicate that there is potential for developing electroactive devices with switchable conductive states.

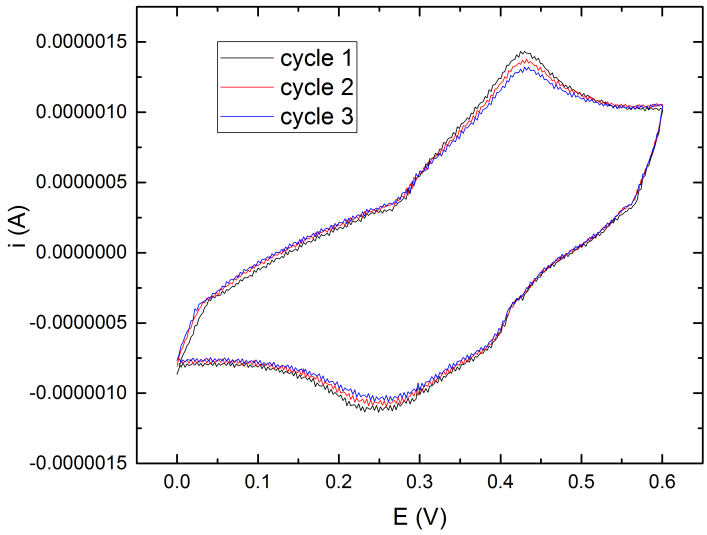

Figure 5.20: CV measurements of hydrogels prepared with a total volume of 15 mL of 3 parts of 0.2% CNF one part of 0.2% TAN with 0.5% GdL. Scan rate 100 mV/s.

Chapter 6

Conclusions

Hydrogels were prepared from CNF colloidal suspensions by a timing, based on chemical programming. It was implemented by controlling the GdL hydrolysis rate which depends on its aqueous concentration. The rheological measurements indicated that the storage modulus increases as a function of increased GdL concentration, leading to the protonation of the TEMPO-oxidized CNF to the carboxylic acid states from the initial sodium-salt state. This increase of hydrophobic interactions and hydrogen bonds beyween CNFs to produce gels. The GdL amount allows also to control the kinetics of the gelation.

The protonation state of CNF was detected spectroscopically. It also allowed to detect the time evolution.

The chemical programming enabled to introduce conjugated units in the hydrogels in a solution based approach, which allowed a processing window to prepare composite hydrogels with controlled compositions. Hydrogels were produced with different electroactive components such as CNT and TANI. The hydrogels prepared with CNT showed anisotropy.

The chemical programming has potential to construct even more complex networks. We suggest the use of two colloidal building blocks with different responses, for example, acidities (pKa). The differences in pKa of the components will lead to sequential formation of networks at different times. The final aim is to produce two independent self-sorted networks based on the differences in pKa avoiding phase segregation. For example, double gels are foreseen, depicted in the literature as a way of producing anisotropic materials with excellent mechanical properties [115, 116].

Monitoring of gelation was made possible with the help of organic dyes. It would be interesting to see the effect of such dyes on the self-assembly of fibrils in combination with organic semiconductors such as TANI.

The chemical programming of gels with CNF gels has potential for

producing components at different length scales. This can be implemented in combination with new fabrication methods which requires control over the viscosity of the materials. Hydrogels of different geometries in combination with organic semiconductors finds applications in stretchable electronics such as electrodes and batteries [117, 118].

The produced hydrogels enabled the in-situ electrochemical characterizations of conductive materials. The preliminary electrochemical results indicate that CNF hydrogels can be used as electrochemical medium for carrying out redox reactions. This could allow in-situ chemical reaction, for example, reduction of FWCNTs to further enhance the conductivity.

The conductivity exhibited by the hydrogels includes both electronic and ionic components. It would be interesting to segregate both the components to find the ionic conductivity of the gels with better impedance models. Finally, the produced hydrogels have potential for developing various iontronic devices such as diodes and transistors [119, 120]. One can also envision complex circuits consisting of redox sensitive polymers to fabricate electrochromic devices [121].

Bibliography

[1] Dan Gavrilescu. Energy from biomass in pulp and paper mills, 2008.

[2] B.-J. de.Gans, P.C. Duineveld, and U.S. Schubert. Inkjet Printing of Polymers: State of the Art and Future Developments. *Advanced Materials*, 16(3):203–213, 2004.

[3] Allan S. Hoffman. Hydrogels for biomedical applications. *Advanced Drug Delivery Reviews*, 64(SUPPL.):18–23, 2012.

[4] Honggu Chun and Taek Dong Chung. Iontronics. *Annual Review of Analytical Chemistry*, 8(1):441–462, 2015.

[5] Paschalis Gkoupidenis, Nathan Schaefer, Xenofon Strakosas, Jessamyn A. Fairfield, and George G. Malliaras. Synaptic plasticity functions in an organic electrochemical transistor. *Applied Physics Letters*, 107(26):26–31, 2015.

[6] Fabien Alibart, Stéphane Pieutin, David Guérin, Christophe Novembre, Stéphane Lenfant, Kamal Lmimouni, Christian Gamrat, and Dominique Vuillaume. An organic nanoparticle transistor behaving as a biological spiking synapse. *Advanced Functional Materials*, 20(2):330–337, 2010.

[7] Gang Liu, Cheng Wang, Wenbin Zhang, Liang Pan, Chaochao Zhang, Xi Yang, Fei Fan, Yu Chen, and Run-Wei Li. Organic biomimicking memristor for information storage and processing applications. *Advanced Electronic Materials*, 2(2), 2016.

[8] Peng Lin and Feng Yan. Organic thin-film transistors for chemical and biological sensing. *Advanced Materials*, 24(1):34–51, 2012.

[9] Kezheng Gao, Ziqiang Shao, Jia Li, Xi Wang, Xiaoqing Peng, Wenjun Wang, and Feijun Wang. Cellulose nanofiberâgraphene all solid-state flexible supercapacitors. *J. Mater. Chem. A*, 1(1):63–67, 2013.

[10] Usman Ali Rana, Maria Forsyth, Douglas R. Macfarlane, and Jennifer M. Pringle. Toward protic ionic liquid and organic ionic plastic crystal electrolytes for fuel cells. *Electrochimica Acta*, 84:213–222, 2012.

[11] Mariana Díaz, Alfredo Ortiz, and Inmaculada Ortiz. Progress in the use of ionic liquids as electrolyte membranes in fuel cells. *Journal of Membrane Science*, 469:379–396, 2014.

[12] Mihai Irimia-Vladu. Green electronics: biodegradable and biocompatible materials and devices for sustainable future. *Chem. Soc. Rev.*, 43(2):588–610, feb 2014.

[13] Suthipong Sthiannopkao and Ming Hung Wong. Handling e-waste in developed and developing countries: Initiatives, practices, and consequences. *Science of the Total Environment*, 463-464:1147–1153, 2013.

[14] Vijay Kumar Garlapati. E-waste in India and developed countries: Management, recycling, business and biotechnological initiatives. *Renewable and Sustainable Energy Reviews*, 54:874–881, 2016.

[15] Shaoting Lin, Hyunwoo Yuk, Teng Zhang, German Alberto Parada, Hyunwoo Koo, Cunjiang Yu, and Xuanhe Zhao. Stretchable Hydrogel Electronics and Devices. *Advanced Materials*, 28(22):4497–4505, 2016.

[16] Yun Jung Heo and Shoji Takeuchi. Towards Smart Tattoos: Implantable Biosensors for Continuous Glucose Monitoring. *Advanced Healthcare Materials*, 2(1):43–56, 2013.

[17] Lucia Kidalova, Nadezda Stevulova, Eva Terpakova, and Alena Sicakova. Utilization of alternative materials in lightweight composites. *Journal of Cleaner Production*, 34(October):116–119, 2012.

[18] Nicholas A. Hoenich. Cellulose for Medical Applications: Past, Present, and Future. *BioResources*, 1(2):270–280, 2007.

[19] Yei Hwan Jung, Tzu-Hsuan Chang, Huilong Zhang, Chunhua Yao, Qifeng Zheng, Vina W Yang, Hongyi Mi, Munho Kim, Sang June Cho, Dong-Wook Park, Hao Jiang, Juhwan Lee, Yijie Qiu, Weidong Zhou, Zhiyong Cai, Shaoqin Gong, and Zhenqiang Ma. High-performance green flexible electronics based on biodegradable cellulose nanofibril paper. *Nature communications*, 6(May):7170, 2015.

[20] H. Sirringhaus, P. J. Brown, R. H. Friend, M. M. Nielsen, K. Bechgaard, B. M. W. Langeveld-Voss, a. J. H. Spiering, R. a. J. Janssen, E. W. Meijer, P. Herwig, and D. M. de Leeuw. Two-Dimensional Charge Transport in Self-Organized, High-Mobility Conjugated Polymers. *Nature*, 401(6754):685–688, 1999.

[21] Lehn (VCH) VonJ.-M. *Supramolecular Chemistry. Concepts and Perspectives.*, volume 107. 1995.

[22] Philippe Cordier, François Tournilhac, Corinne Soulié-Ziakovic, and Ludwik Leibler. Self-healing and thermoreversible rubber from supramolecular assembly. *Nature*, 451(7181):977–80, 2008.

[23] Emma Rose Janeček, Jason R. McKee, Cindy S Y Tan, Antti Nykänen, Marjo Kettunen, Janne Laine, Olli Ikkala, and Oren A. Scherman. Hybrid supramolecular and colloidal hydrogels that bridge multiple length scales. *Angewandte Chemie - International Edition*, 54(18):5383–5388, 2015.

[24] Alain Dufresne. Polymer Nanocomposites from Biological Sources. *Encyclopedia of Nanoscience and Nanotechnology*, (January 2007):1–32, 2009.

[25] Dieter Klemm, Brigitte Heublein, Hans Peter Fink, and Andreas Bohn. Cellulose: Fascinating biopolymer and sustainable raw material. *Angewandte Chemie - International Edition*, 44(22):3358–3393, 2005.

[26] Gilberto Siqueira, Julien Bras, and Alain Dufresne. Cellulosic bionanocomposites: A review of preparation, properties and applications, 2010.

[27] Robert J Moon, Ashlie Martini, John Nairn, John Simonsen, and Jeff Youngblood. Cellulose nanomaterials review: structure, properties and nanocomposites. *Chemical Society Reviews*, 40(7):3941, 2011.

[28] Youssef Habibi, Lucian A. Lucia, and Orlando J. Rojas. Cellulose nanocrystals: Chemistry, self-assembly, and applications. *Chemical Reviews*, 110(6):3479–3500, 2010.

[29] Akira Isogai, Tsuguyuki Saito, and Hayaka Fukuzumi. TEMPO-oxidized cellulose nanofibers. *Nanoscale*, 3(1):71–85, 2011.

[30] Tsuguyuki Saito, Satoshi Kimura, Yoshiharu Nishiyama, and Akira Isogai. Cellulose nanofibers prepared by TEMPO-mediated oxidation of native cellulose. *Biomacromolecules*, 8(8):2485–2491, 2007.

[31] István Siró and David Plackett. Microfibrillated cellulose and new nanocomposite materials: a review. *Cellulose*, 17(3):459–494, 2010.

[32] Carlos Salas, Tiina Nypelö, Carlos Rodriguez-Abreu, Carlos Carrillo, and Orlando J. Rojas. Nanocellulose properties and applications in colloids and interfaces, 2014.

[33] G. M. Whitesides. Self-Assembly at All Scales. *Science*, 295(5564):2418–2421, 2002.

[34] Bartosz a. Grzybowski, Christopher E. Wilmer, Jiwon Kim, Kevin P. Browne, and Kyle J. M. Bishop. Self-assembly: from crystals to cells. *Soft Matter*, 5(6):1110, 2009.

[35] Lenny Voorhaar and Richard Hoogenboom. Supramolecular polymer networks: hydrogels and bulk materials. *Chemical Society Reviews*, 45(14):4013–4031, 2016.

[36] Emily E Meyer, Kenneth J Rosenberg, and Jacob Israelachvili. Recent progress in understanding hydrophobic interactions. *Proceedings of the National Academy of Sciences of the United States of America*, 103(43):15739–15746, 2006.

[37] Bruno Medronho, Anabela Romano, Maria Graça Miguel, Lars Stigsson, and Björn Lindman. Rationalizing cellulose (in)solubility: Reviewing basic physicochemical aspects and role of hydrophobic interactions. *Cellulose*, 19(3):581–587, 2012.

[38] Margaret C. Etter. Encoding and decoding hydrogen-bond patterns of organic compounds. *Accounts of Chemical Research*, 23(4):120–126, 1990.

[39] G. Gilli and P. Gilli. Towards an unified hydrogen-bond theory. In *Journal of Molecular Structure*, volume 552, pages 1–15, 2000.

[40] Woo-jin Jeong, Sanghun Han, Hyeseo Park, Kyeong Sik Jin, and Yong-beom Lim. Multiplexing natural orientation: Oppositely directed self-assembling peptides. *Biomacromolecules*, 15(6):2138–2145, 2014.

[41] J. Emsley. Very strong hydrogen bonding. *Chemical Society Reviews*, 9(1):91, 1980.

[42] Björn Lindman, Gunnar Karlström, and Lars Stigsson. On the mechanism of dissolution of cellulose. *Journal of Molecular Liquids*, 156(1):76–81, 2010.

[43] Miao Wang, Anna Olszewska, Andreas Walther, Jani Markus Malho, Felix H. Schacher, Janne Ruokolainen, Mikael Ankerfors, Janne Laine, Lars A. Berglund, Monika Österberg, and Olli Ikkala. Colloidal ionic assembly between anionic native cellulose nanofibrils and cationic block copolymer micelles into biomimetic nanocomposites. *Biomacromolecules*, 12(6):2074–2081, 2011.

[44] Jia Huang, Hongli Zhu, Yuchen Chen, Colin Preston, Kathleen Rohrbach, John Cumings, and Liangbing Hu. Highly transparent and flexible nanopaper transistors. *ACS Nano*, 7(3):2106–2113, 2013.

[45] Enas M. Ahmed. Hydrogel: Preparation, characterization, and applications: A review. *Journal of Advanced Research*, 6(2):105–121, 2015.

[46] Matti S Toivonen, Antti Kaskela, Orlando J Rojas, Esko I Kauppinen, and Olli Ikkala. Ambient-dried cellulose nanofibril aerogel membranes with high tensile strength and their use for aerosol collection and templates for transparent, flexible devices. *Advanced Functional Materials*, 25(42):6618–6626, 2015.

[47] M. Pääkko, M. Ankerfors, H. Kosonen, A. Nykänen, S. Ahola, M. Österberg, J. Ruokolainen, J. Laine, P. T. Larsson, Olli Ikkala, and T. Lindström. Enzymatic hydrolysis combined with mechanical shearing and high-pressure homogenization for nanoscale cellulose fibrils and strong gels. *Biomacromolecules*, 8(6):1934–1941, 2007.

[48] Tsuguyuki Saito, Takehiko Uematsu, Satoshi Kimura, Toshiharu Enomae, and Akira Isogai. Self-aligned integration of native cellulose nanofibrils towards producing diverse bulk materials. *Soft Matter*, 7(19):8804, 2011.

[49] Hong Dong, James F. Snyder, Kristen S. Williams, and Jan W. Andzelm. Cation-induced hydrogels of cellulose nanofibrils with tunable moduli. *Biomacromolecules*, 14(9):3338–3345, 2013.

[50] Hong Dong, James F. Snyder, Dat T. Tran, and Julia L. Leadore. Hydrogel, aerogel and film of cellulose nanofibrils functionalized with silver nanoparticles. *Carbohydrate Polymers*, 95(2):760–767, 2013.

[51] Juuso T. Korhonen, Panu Hiekkataipale, Jari Malm, Maarit Karppinen, Olli Ikkala, and Robin H A Ras. Inorganic hollow nanotube aerogels by atomic layer deposition onto native nanocellulose templates. *ACS Nano*, 5(3):1967–1974, 2011.

[52] Hao Jin, Yoshiharu Nishiyama, Masahisa Wada, and Shigenori Kuga. Nanofibrillar cellulose aerogels. *Colloids and Surfaces A: Physicochemical and Engineering Aspects*, 240(1-3):63–67, 2004.

[53] Zhen Yu Wu, Chao Li, Hai Wei Liang, Jia Fu Chen, and Shu Hong Yu. Ultralight, flexible, and fire-resistant carbon nanofiber aerogels from bacterial cellulose. *Angewandte Chemie - International Edition*, 52(10):2925–2929, 2013.

[54] Maria Dolores Segarra-Maset, Vicent J Nebot, Juan F Miravet, and Beatriu Escuder. Control of molecular gelation by chemical stimuli. *Chemical Society reviews*, 42(17):7086–98, 2013.

[55] Jaclyn Raeburn, Andre Zamith Cardoso, and Dave J Adams. The importance of the self-assembly process to control mechanical properties of low molecular weight hydrogels. *Chem. Soc. Rev.*, 42(12):5143–5156, 2013.

[56] S Ramachandran, P Fontanille, A Pandey, and C Larroche. Gluconic Acid: Properties, Applications and Microbial Production. *Food Technology and Biotechnology*, 44(2):185–195, 2006.

[57] Sneha A Parke, Gordon G Birch, Douglas B Macdougall, and David A Stevens. Tastes , Structure and Solution Properties of.

[58] Y Pocker and Edmond Green. Hydrolysis of D-glucono-δ-lactone. I. General acid-base catalysis, solvent deuterium isotope effects, and transition state characterization. *J. Amer. Chem. Soc.*, 95(Copyright (C) 2012 American Chemical Society (ACS). All Rights Reserved.):113–119, 1973.

[59] Dave J. Adams, Michael F. Butler, William J. Frith, Mark Kirkland, Leanne Mullen, and Paul Sanderson. A new method for maintaining homogeneity during liquidâhydrogel transitions using low molecular weight hydrogelators. *Soft Matter*, 5(9):1856, 2009.

[60] Andre Zamith Cardoso, Ana Estefania Alvarez Alvarez, Beatrice N. Cattoz, Peter C. Griffiths, Stephen M. King, William J. Frith, and Dave J. Adams. The influence of the kinetics of self-assembly on the

properties of dipeptide hydrogels. *Faraday Discussions*, 166(0):101, 2013.

[61] Dennis Go, Thomas E. Kodger, Joris Sprakel, and Alexander Kuehne. Programmable co-assembly of oppositely charged microgels. *Soft Matter*, 10:8060–8065, 2014.

[62] Yury Shchipunov, Nadya Ivanova, and Vladimir Silant'ev. Bionanocomposites formed by in situ charged chitosan with clay. *Green Chemistry*, 11(11):1758–1761, 2009.

[63] Thomas Heuser, Ann Kathrin Steppert, Catalina Molano Lopez, Baolei Zhu, and Andreas Walther. Generic Concept to Program the Time Domain of Self-Assemblies with a Self-Regulation Mechanism. *Nano Letters*, 15(4):2213–2219, 2015.

[64] Kwang J Kim and Satoshi Tadokoro. *Electroactive Polymers for Robotic Applications*, volume 93. 2007.

[65] Zheng Chen, John W F To, Chao Wang, Zhenda Lu, Nan Liu, Alex Chortos, Lijia Pan, Fei Wei, Yi Cui, and Zhenan Bao. A three-dimensionally interconnected carbon nanotube-conducting polymer hydrogel network for high-performance flexible battery electrodes. *Advanced Energy Materials*, 4(12), 2014.

[66] H W Heuer, R Wehrmann, and S Kirchmeyer. Electrochromic window based on conducting poly (3,4-ethylenedioxythiophene)poly(styrene sulfonate). *Advanced Functional Materials*, 12(2):89–94, 2002.

[67] Anthony Guiseppi-Elie. Electroconductive hydrogels: Synthesis, characterization and biomedical applications. *Biomaterials*, 31(10):2701–2716, 2010.

[68] S Ghosh and O Inganäs. Conducting Polymer Hydrogels as 3D Electrodes: Applications for Supercapacitors. *Advanced Materials*, 11(14):1214–1218, 1999.

[69] Rylie A Green, Sungchul Baek, Laura A Poole-Warren, and Penny J Martens. Conducting polymer-hydrogels for medical electrode applications. *Sci. Technol. Adv. Mater. Sci. Technol. Adv. Mater*, 11(11):14107–13, 2010.

[70] Lanlan Li, Ye Shi, Lijia Pan, Yi Shi, and Guihua Yu. Rational design and applications of conducting polymer hydrogels as electrochemical biosensors. *Journal of Materials Chemistry B*, 3(15):2920–2930, 2015.

[71] Yu Zhao, Borui Liu, Lijia Pan, and Guihua Yu. 3D nanostructured conductive polymer hydrogels for high-performance electrochemical devices. *Energy & Environmental Science*, 6(10):2856, 2013.

[72] Damia Mawad, Elise Stewart, David L. Officer, Tony Romeo, Pawel Wagner, Klaudia Wagner, and Gordon G. Wallace. A single component conducting polymer hydrogel as a scaffold for tissue engineering. *Adv. Funct. Mater.*, 22(13):2692–2699, 2012.

[73] James F Beecher. Organic materials: Wood, trees and nanotechnology. *Nature Nanotechnology*, 2(8):466–467, 2007.

[74] Rira Jung, Hun Sik Kim, Yeseul Kim, Soon Min Kwon, Heon Sang Lee, and Hyoung Joon Jin. Electrically conductive transparent papers using multiwalled carbon nanotubes. *Journal of Polymer Science, Part B: Polymer Physics*, 46(12):1235–1242, 2008.

[75] Lijia Pan, Guihua Yu, Dongyuan Zhai, Hye Ryoung Lee, Wenting Zhao, Nian Liu, Huiliang Wang, Benjamin C-K Tee, Yi Shi, Yi Cui, and Zhenan Bao. Hierarchical nanostructured conducting polymer hydrogel with high electrochemical activity. *Proceedings of the National Academy of Sciences of the United States of America*, 109(24):9287–92, 2012.

[76] Zhijun Shi, Xing Gao, Muhammad Wajid Ullah, Sixiang Li, Qun Wang, and Guang Yang. Electroconductive natural polymer-based hydrogels. *Biomaterials*, (October), 2016.

[77] Miao Wang, Ilya V. Anoshkin, Albert G. Nasibulin, Robin H. A. Ras, Nonappa Nonappa, Janne Laine, Esko I. Kauppinen, and Olli Ikkala. Electrical behaviour of native cellulose nanofibril/carbon nanotube hybrid aerogels under cyclic compression. *RSC Adv.*, 6(92):89051–89056, 2016.

[78] Jean Roncali. Conjugated poly(thiophenes): synthesis, functionalization, and applications. *Chemical Reviews*, 92(4):711–738, 1992.

[79] Xiaodan Zhang, Ziyin Lin, Bo Chen, Wei Zhang, Sudhir Sharma, Wentian Gu, and Yulin Deng. Solid-state flexible polyaniline/silver cellulose nanofibrils aerogel supercapacitors. *Journal of Power Sources*, 246:283–289, 2014.

[80] Dongfang Qiu, Yanxiang Cheng, and Lixiang Wang. Oligoaniline-functionalized terpyridine ligands and their ruthenium(II) complexes: synthesis, spectroscopic property and redox behavior. *Dalton transactions (Cambridge, England : 2003)*, (17):3247–61, 2009.

[81] Zhixiang Wei and Charl F J Faul. Aniline oligomers - Architecture, function and new opportunities for nanostructured materials. *Macromolecular Rapid Communications*, 29(4):280–292, 2008.

[82] Yue Wang, Henry D. Tran, Lei Liao, Xiangfeng Duan, and Richard B. Kaner. Nanoscale morphology, dimensional control, and electrical properties of oligoanilines. *Journal of the American Chemical Society*, 132(30):10365–10373, 2010.

[83] Thomas G. Dane, Philip T. Cresswell, Oier Bikondoa, Gemma E. Newby, Thomas Arnold, Charl F. J. Faul, and Wuge H. Briscoe. Structured oligo(aniline) nanofilms via ionic self-assembly. *Soft Matter*, 8(10):2824–2832, 2012.

[84] Erik T Thostenson, Zhifeng Ren, and Tsu-Wei Chou. Advances in the science and technology of carbon nanotubes and their composites: a review. *Composites Science and Technology*, 61(13):1899–1912, 2001.

[85] Sumio Iijima. Helical microtubules of graphitic carbon. *Nature*, 354:56–58, 1991.

[86] J.-P. Salvetat, J.-M. Bonard, N.H. Thomson, A.J. Kulik, L. Forro;, W. Benoit, and L. Zuppiroli. Mechanical properties of carbon nanotubes. *Applied Physics A: Materials Science & Processing*, 69(3):255–260, 1999.

[87] P J F Harris. Carbon nanotube composites. *International Materials Reviews*, 49(1):31–43, 2004.

[88] Nguyen Tran Hung, I. V. Anoshkin, A. P. Dementjev, D. V. Katorov, and E. G. Rakov. Functionalization and solubilization of thin multiwalled carbon nanotubes. *Inorganic Materials*, 44(3):219–223, 2008.

[89] Jinyong Wang, Haibin Chu, and Yan Li. Why single-walled carbon nanotubes can be dispersed in imidazolium-based ionic liquids. *ACS Nano*, 2(12):2540–2546, 2008.

[90] Linda Vaisman, H. Daniel Wagner, and Gad Marom. The role of surfactants in dispersion of carbon nanotubes. *Advances in Colloid and Interface Science*, 128-130(2006):37–46, 2006.

[91] Miao Wang, Ilya V. Anoshkin, Albert G. Nasibulin, Juuso T. Korhonen, Jani Seitsonen, Jaakko Pere, Esko I. Kauppinen, Robin H A Ras, and Olli Ikkala. Modifying native nanocellulose aerogels with carbon nanotubes for mechanoresponsive conductivity and pressure sensing. *Advanced Materials*, 25(17):2428–2432, 2013.

[92] Sedat Ondaral, Guliz Hocaoglu, and Mehmet Emin Ergun. Cationic and anionic nanofibrillated celluloses as dry stregth additives for papermaking. *CELLULOSE CHEMISTRY AND TECHNOLOGY*, 49(7-8):617–623, 2015.

[93] Zhecheng Shao, Patrice Rannou, Saïd Sadki, Natalie Fey, David M Lindsay, and Charl FJ Faul. Delineating poly (aniline) redox chemistry by using tailored oligo (aryleneamine) s: Towards oligo (aniline)-based organic semiconductors with tunable optoelectronic properties. *Chemistry-A European Journal*, 17(44):12512–12521, 2011.

[94] Richard G. Weiss and Pierre Terech. *Molecular gels: Materials with self-assembled fibrillar networks*. 2006.

[95] Yasir Beeran P. T., Vid Bobnar, Selestina Gorgieva, Yves Grohens, Matjaž Finšgar, Sabu Thomas, and Vanja Kokol. Mechanically strong, flexible and thermally stable graphene oxide/nanocellulosic films with enhanced dielectric properties. *RSC Adv.*, 6(54):49138–49149, 2016.

[96] Feng Jiang and You-Lo Hsieh. Self-assembling of TEMPO Oxidized Cellulose Nanofibrils As Affected by Protonation of Surface Carboxyls and Drying Methods. *ACS Sustainable Chemistry & Engineering*, 4(3):1041–1049, mar 2016.

[97] Madeleine Djabourov, Jacques Leblond, and Pierre Papon. Gelation of aqueous gelatin solutions. II. Rheology of the sol-gel transition. *Journal de Physique*, 49(2):333–343, 1988.

[98] Jonathan M. Zuidema, Christopher J. Rivet, Ryan J. Gilbert, and Faith A. Morrison. A protocol for rheological characterization of hydrogels for tissue engineering strategies. *Journal of Biomedical Materials Research - Part B Applied Biomaterials*, 102(5):1063–1073, 2014.

[99] Andreas B. Fall, Stefan B. Lindström, Joris Sprakel, and Lars Wågberg. A physical cross-linking process of cellulose nanofibril gels with shear-controlled fibril orientation. *Soft Matter*, 9(6):1852, 2013.

[100] Skelte G. Anema. Effect of temperature and rate of acidification on the rheological properties of acid skim milk gels. *Journal of Food Processing and Preservation*, 32(6):1016–1033, 2008.

[101] Todd R. Hoare and Daniel S. Kohane. Hydrogels in drug delivery: Progress and challenges, 2008.

[102] Nguyen Tran Hung, I. V. Anoshkin, A. P. Dementjev, D. V. Katorov, and E. G. Rakov. Functionalization and solubilization of thin multiwalled carbon nanotubes. *Inorganic Materials*, 44(3):219–223, mar 2008.

[103] Etj Nibbering, J Dreyer, and O Kühn. Chapter 7. Vibrational dynamics of hydrogen bonds. *Analysis and Control of Ultrafast Photoinduced Reactions Chemical Physics*, pages 619–687, 2007.

[104] Hillel D. Ephros. Toluidine blue staining. *Journal of Oral and Maxillofacial Surgery*, 62:1, 2004.

[105] Gokul Sridharan and Akhil a Shankar. Toluidine blue: A review of its chemistry and clinical utility. *Journal of oral and maxillofacial pathology : JOMFP*, 16(2):251–5, 2012.

[106] L. D'Ilario and Andrea Martinelli. Toluidine blue: aggregation properties and structural aspects. *Modelling and Simulation in Materials Science and Engineering*, 14:581, 2006.

[107] A Xavier Pradeep Dâmello, T Vijay Sylvester, V Ramya, Frankantony P Britto, Priyanka K Shetty, and Shiny Jasphin. Metachromasia and metachromatic dyes: A review.

[108] Jing Liu, Aihua Zou, and Bozhong Mu. Toluidine blue: Aggregation properties and distribution behavior in surfactin micelle solution. *Colloids and Surfaces B: Biointerfaces*, 75(2):496–500, 2010.

[109] Yue Wang, Henry D Tran, Lei Liao, Xiangfeng Duan, and Richard B Kaner. Nanoscale morphology, dimensional control, and electrical properties of oligoanilines. *Journal of the American Chemical Society*, 132(30):10365–10373, 2010.

[110] Alan G. MacDiarmid and Arthur J. Epstein. Secondary doping in polyaniline. *Synthetic Metals*, 69(1-3):85–92, 1995.

[111] Su-Moon Park and Jung-Suk Yoo. Electrochemical Impedance Spectroscopy for Better Electrochemical Measurements. *Analytical Chemistry*, 75:455 A–461 A, 2003.

[112] Seong Hun Kim, Jong Kuk Choi, and Young Chan Bae. Mechanical properties and ionic conductivity of gel polymer electrolyte based on poly(vinylidene-fluoride-co-hexafluoropropylene). *Journal of Applied Polymer Science*, 81(4):948–956, jul 2001.

[113] Noam Agmon. The Grotthuss mechanism. *Chemical Physics Letters*, 244(5-6):456–462, 1995.

[114] N. a. Choudhury, a. K. Shukla, S. Sampath, and S. Pitchumani. Cross-Linked Polymer Hydrogel Electrolytes for Electrochemical Capacitors. *Journal of The Electrochemical Society*, 153(3):A614, 2006.

[115] Jian Ping Gong. Why are double network hydrogels so tough? *Soft Matter*, 6(12):2583, 2010.

[116] Wei Yang, Hidemitsu Furukawa, and Jian Ping Gong. Highly extensible double-network gels with self-assembling anisotropic structure. *Advanced Materials*, 20(23):4499–4503, 2008.

[117] Chuchu Chen, Chuang Yang, Suiyi Li, and Dagang Li. A three-dimensionally chitin nanofiber/carbon nanotube hydrogel network for foldable conductive paper. *Carbohydrate Polymers*, 134:309–313, 2015.

[118] Tao Chen, Rui Hao, Huisheng Peng, and Liming Dai. High-performance, stretchable, wire-shaped supercapacitors. *Angewandte Chemie - International Edition*, 54(2):618–622, 2015.

[119] J H Han, K B Kim, H C Kim, and T D Chung. Ionic circuits based on polyelectrolyte diodes on a microchip. *Angew Chem Int Ed Engl*, 48(21):3830–3833, 2009.

[120] Arif Kösemen, Sait Eren San, Mustafa Okutan, Zekeriya DoÇ§ruyol, Ahmet Demir, Yusuf Yerli, Büsra Sengez, Engin Basaran, and Faruk Yilmaz. A novel field effect transistor with dielectric polymer gel. *Microelectronic Engineering*, 88(1):17–20, 2011.

[121] Roger J. Mortimer, Aubrey L. Dyer, and John R. Reynolds. Electrochromic organic and polymeric materials for display applications, 2006.

Appendix A

Appendix

A.1 Stress sweep measurements for determining linear viscoelastic limit

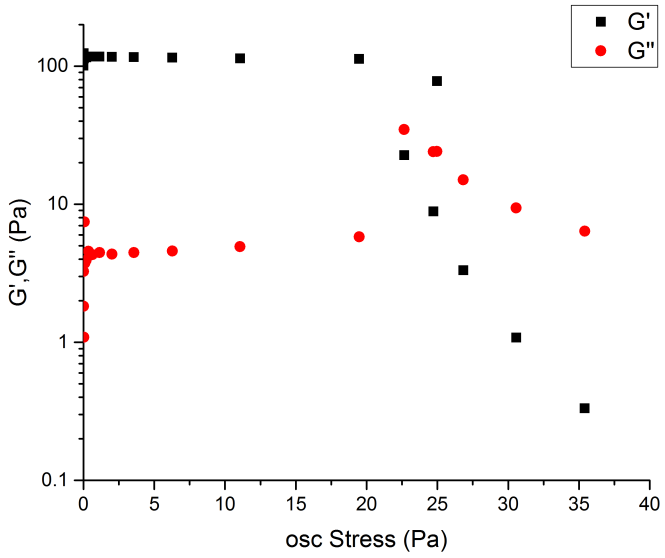

Figure A.1: Stress Sweep of 0.1% TEMPO-CNF gel with 2% GdL at constant angular frequency of 1 rad s^{-1}.

A.2 Mechanical properties of cellulose nanofiber hydrogels

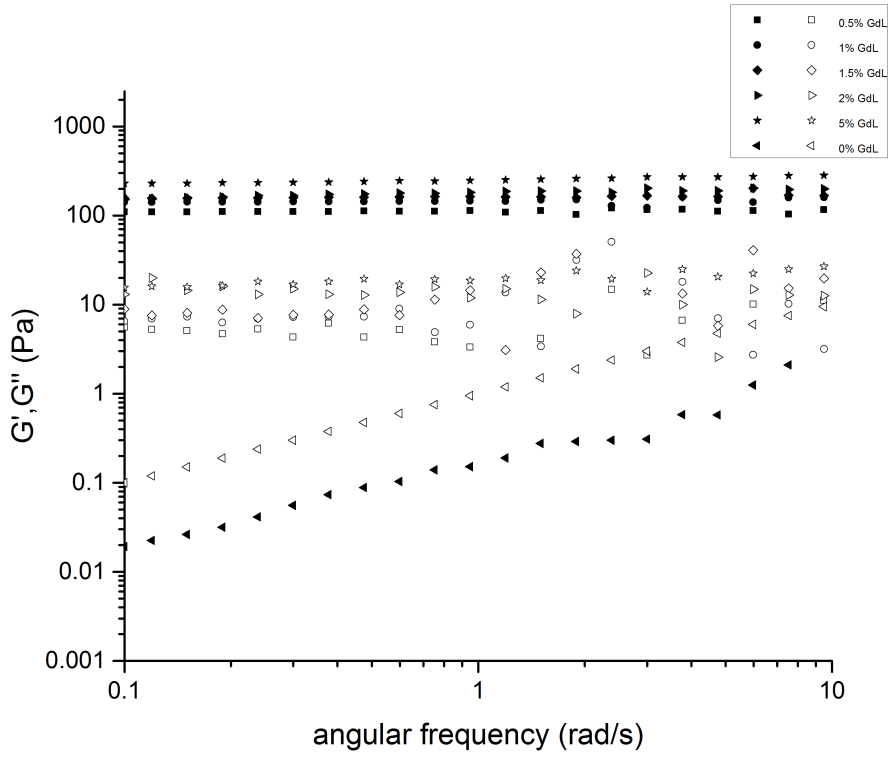

Figure A.2: Storage modulus and loss modulus of 0.1% TEMPO-CNF gels with different GdL concentrations concentrations

A.3 Time sweep measurement of cellulose nanofiber hydrogels

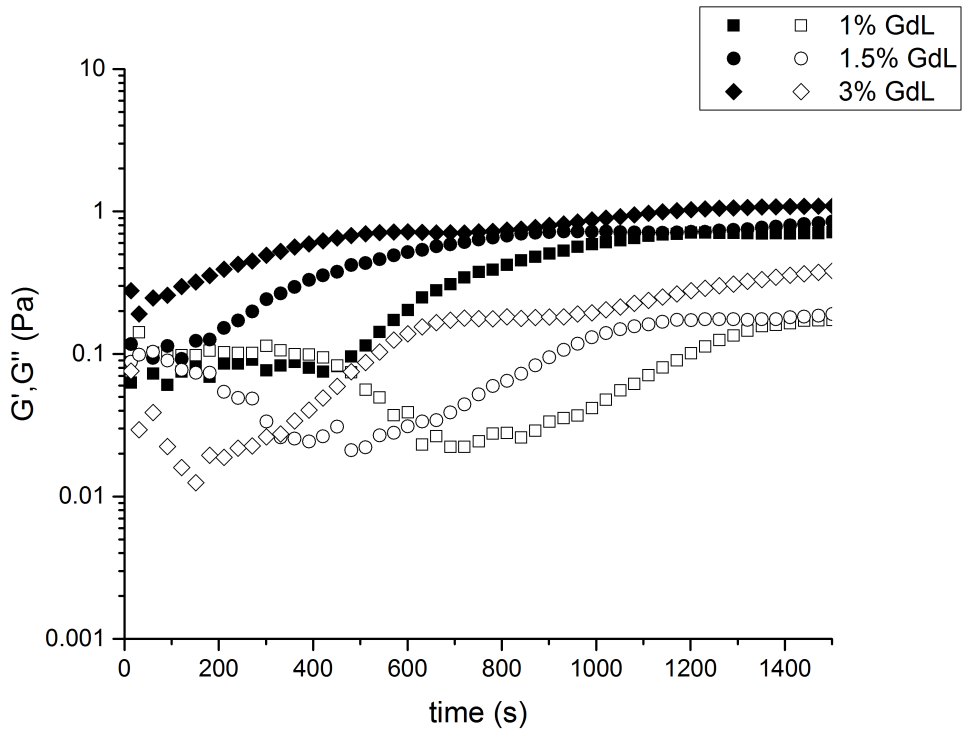

Figure A.3: Time sweep of 0.1% TEMPO CNF at 0.1 Pa oscillatory stress with different GdL concentrations

A.4 Determination of carboxyl content in TEMPO oxidized cellulose nanofiber dispersion

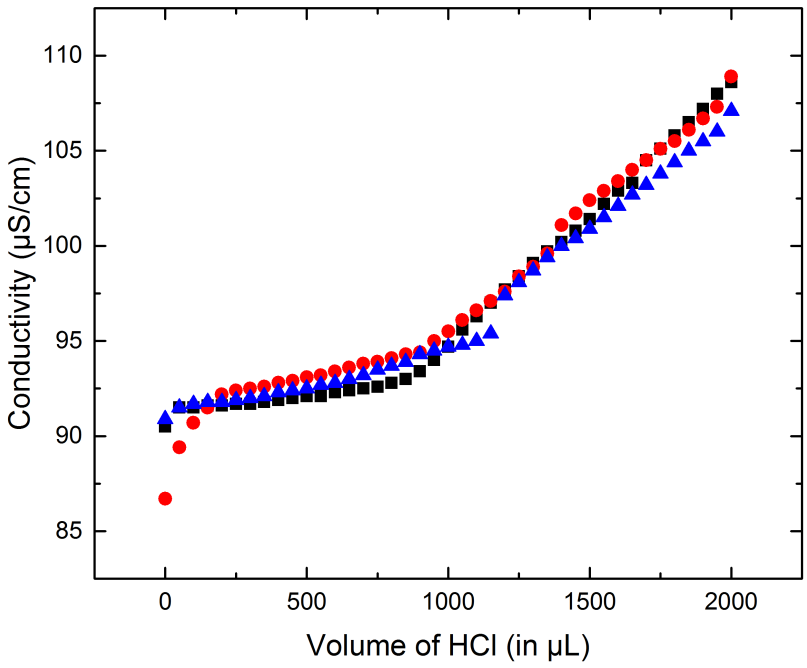

Figure A.4: Conductometric Titration of 0.1% TEMPO-CNF against 0.0285M standardized HCl.

A.5 pH change during glucono-δ-lactone hydrolysis and gelation

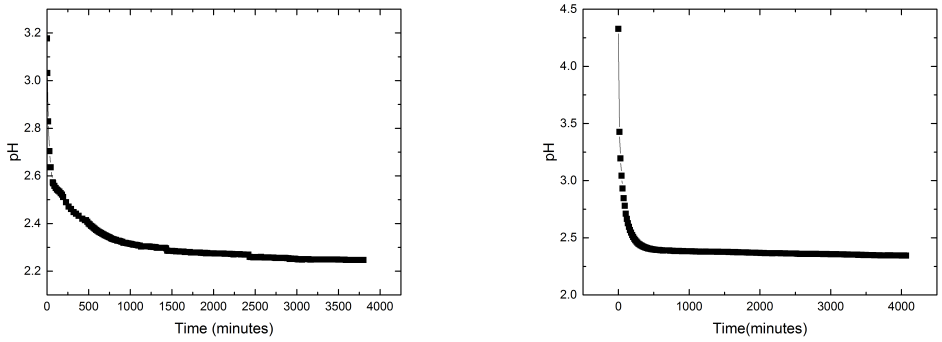

(a) (b)

Figure A.5: (a) Change of pH with time for hydrolysis of 0.75% GdL. (b) Change of pH with time for 0.1% TEMPO-CNF and 0.75% GdL.

A.6 Conductivity measurements during gelation

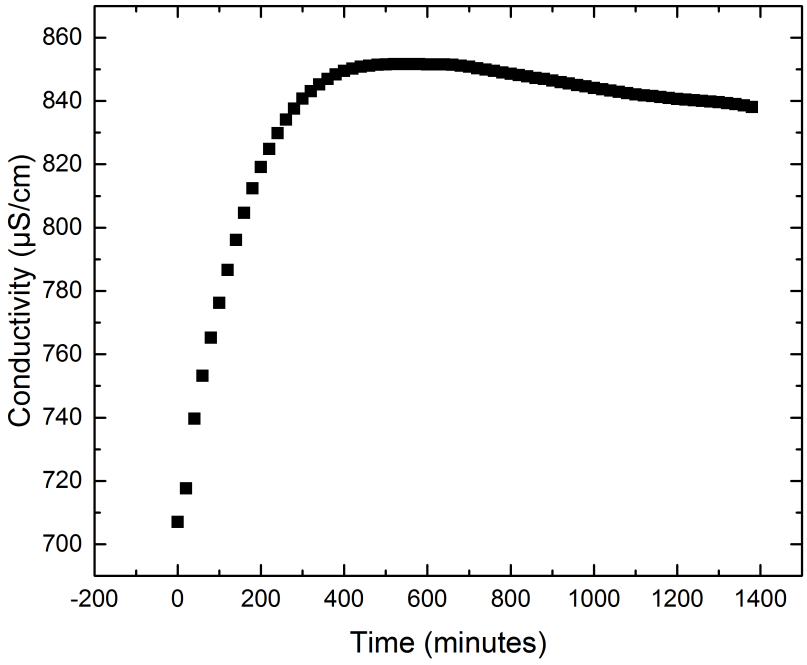

Figure A.6: Conductivity measurements for 0.1% CNF and 0.75% GdL

A.7 Scanning electron microscope of cellulose nanofiber hydrogels

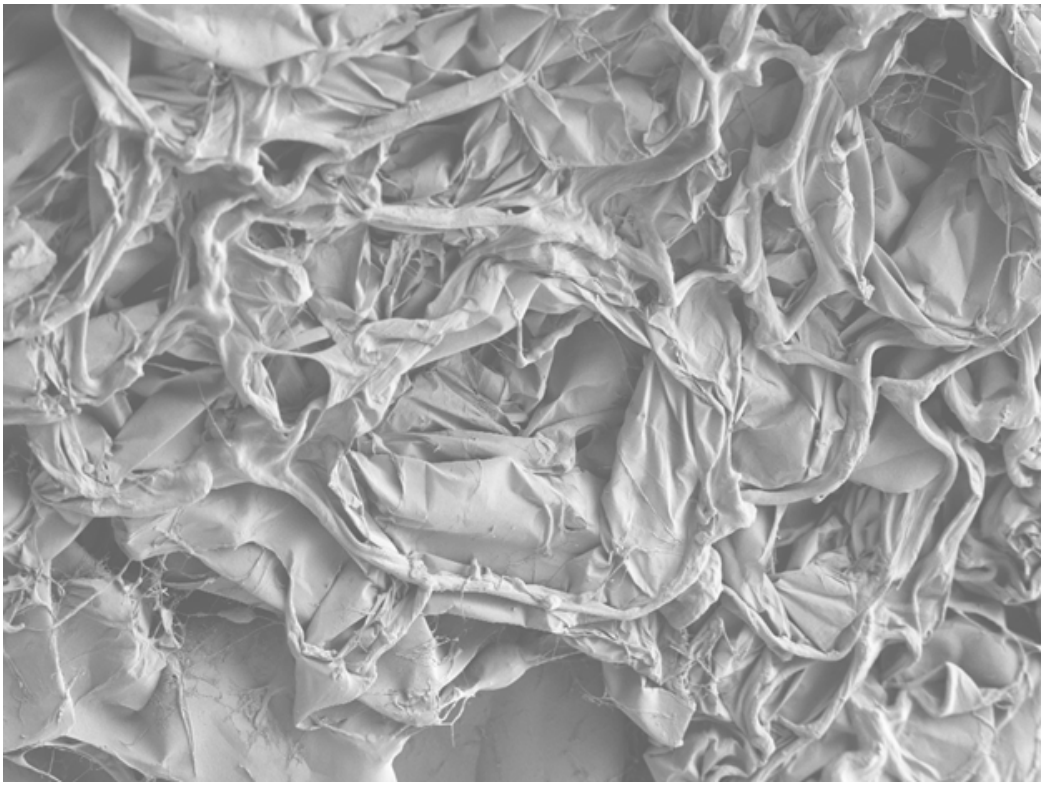

Figure A.7: SEM of 0.25% GdL and 0.1% TEMPO-CNF. The SEM measurements were performed after freeze drying

A.8 Scanning electron microscope of cellulose nanofiber/tetra(aniline) hydrogel with crystals of tetra(aniline)

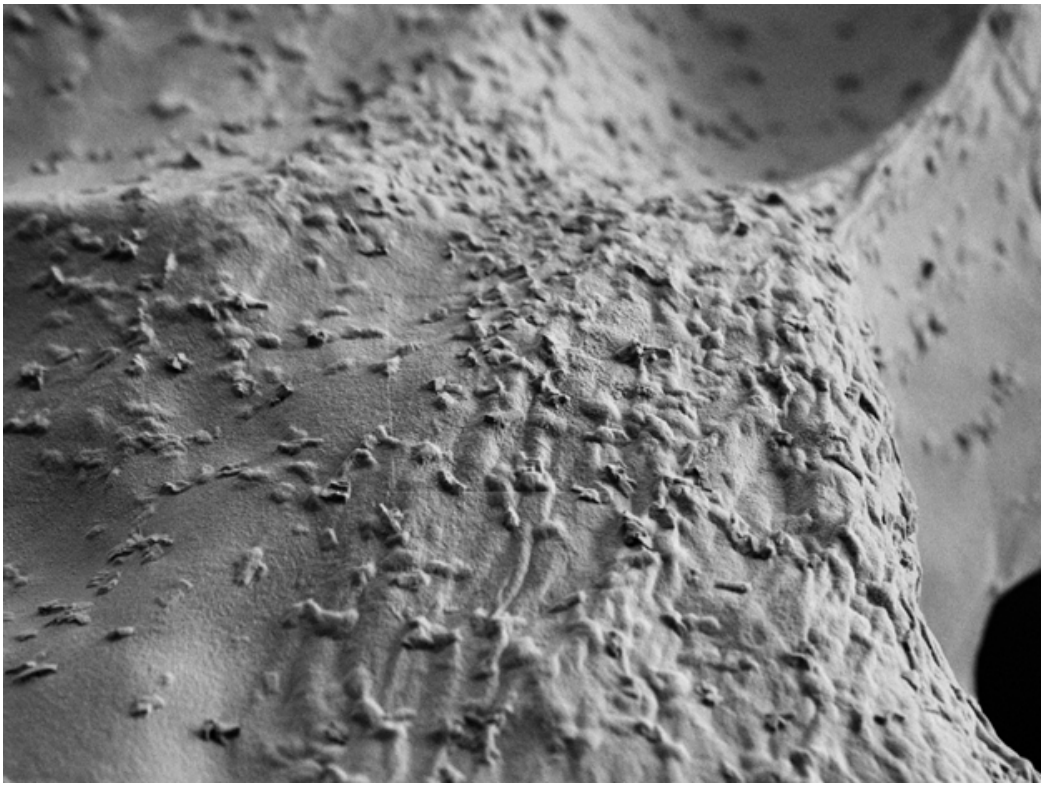

Figure A.8: SEM of 0.2% TEMPO-CNF 0.2% TANI and 2% GdL. The observed big crystals denotes TANI

A.9 Scanning electron microscope of cellulose nanofiber/tetra(aniline) hydrogels

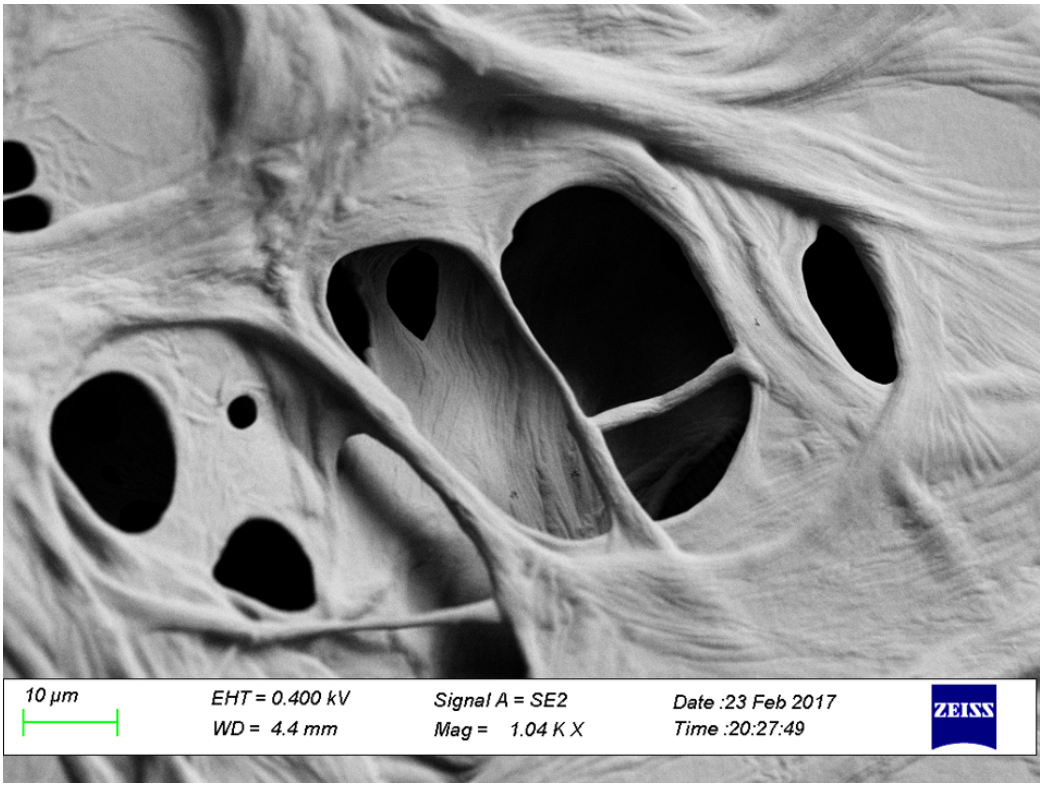

Figure A.9: SEM of 0.2% TEMPO-CNF 0.2% TANI and 0.5% GdL. The gel consists of 25% TANI and 75% CNF

A.10 Transmission electron microscope of cellulose nanofiber dispersion

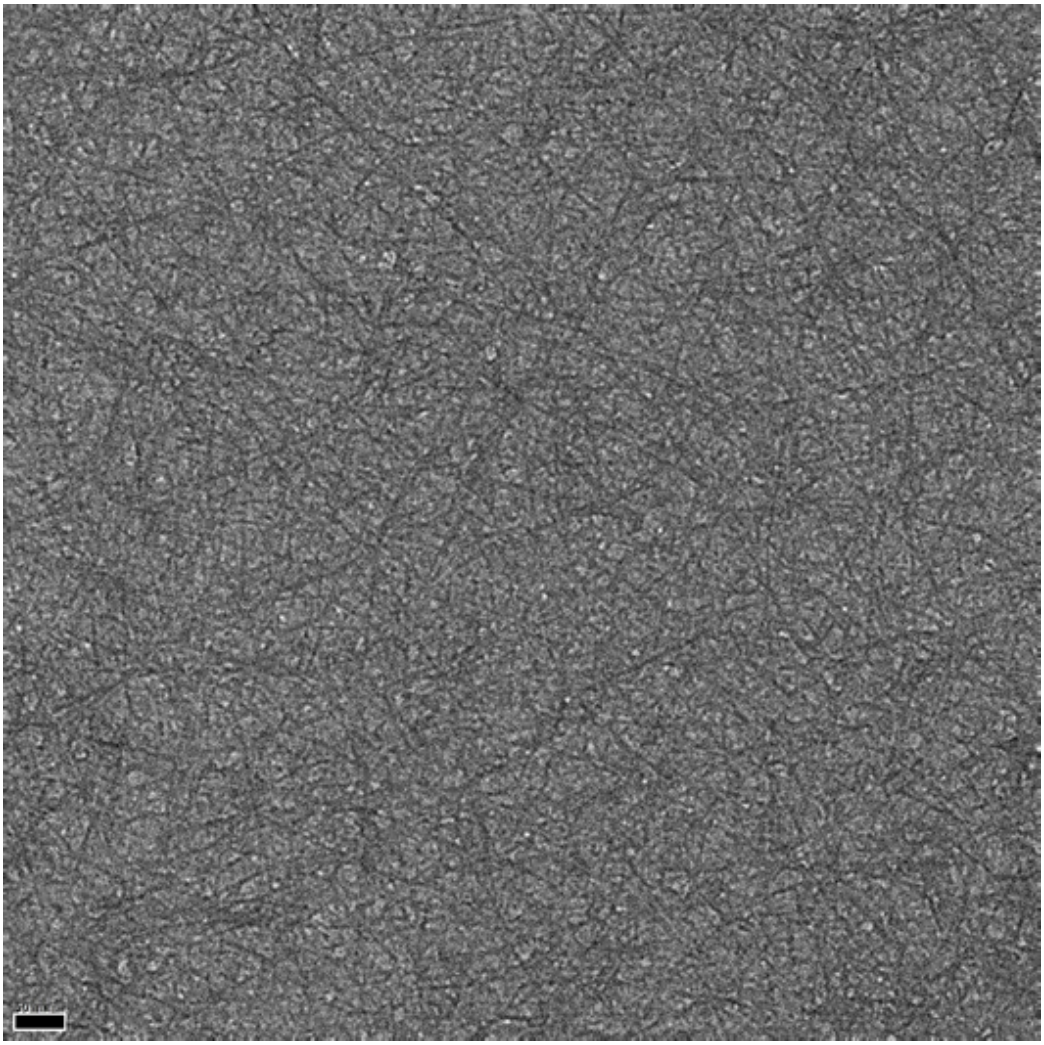

Figure A.10: TEM of 0.1% TEMPO-CNF dispersion. The images were taken after drying the dispersion for two days.

A.11 Transmission electron microscope of cellulose nanofiber gels with toluidine blue

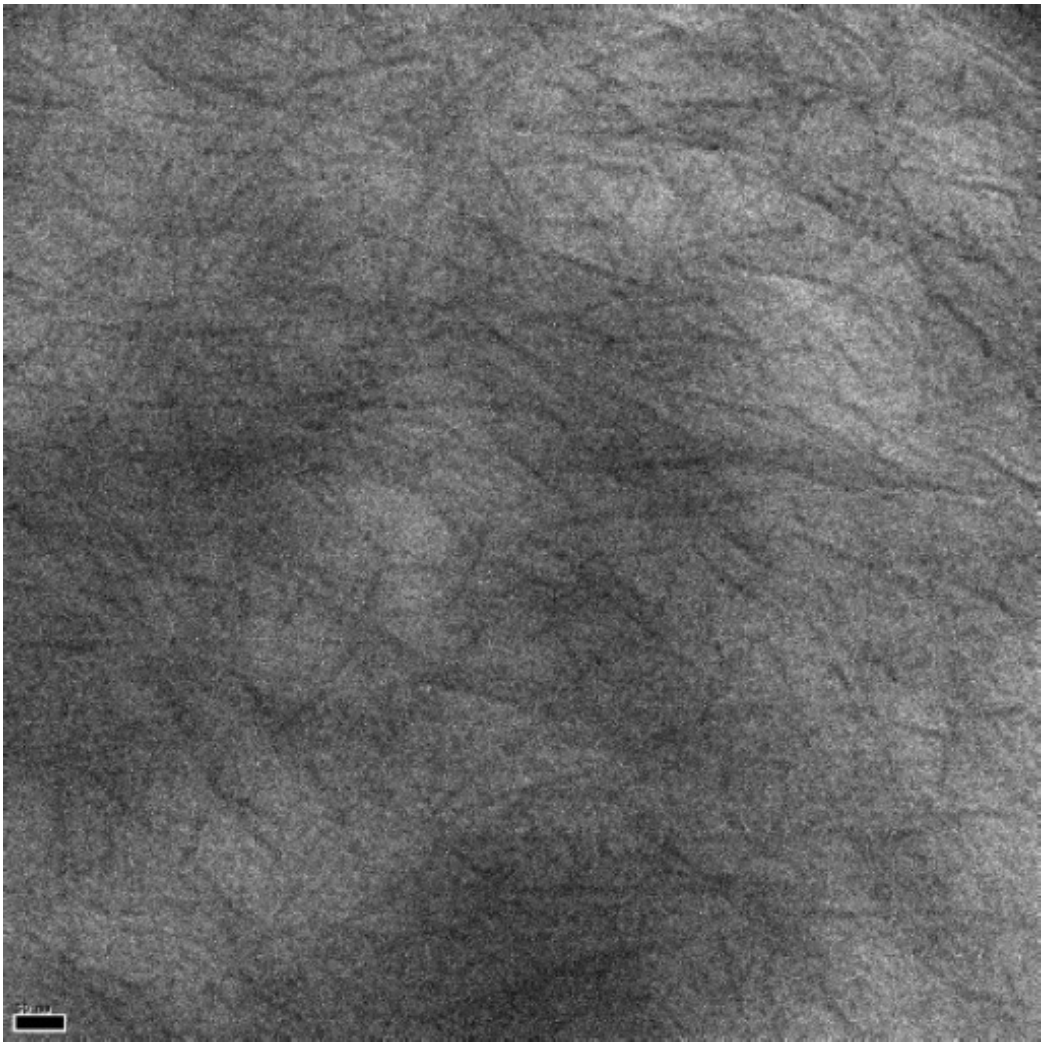

Figure A.11: TEM of 0.1% CNF 2% GdL and 0.0001% TB. The images were taken after drying the gels for two days.